

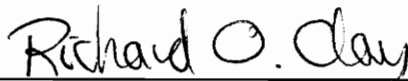
**HIGH RESOLUTION OPTICAL TIME DOMAIN METHODS  
FOR MEASURING STRAIN**

by

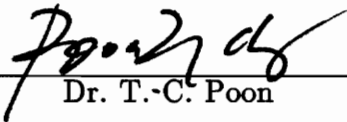
Daniel D. Thomas

Thesis submitted to the Faculty of the  
Virginia Polytechnic Institute and State University  
in partial fulfillment of the requirements for the degree of  
**MASTER OF SCIENCE**  
in  
Electrical Engineering

APPROVED:

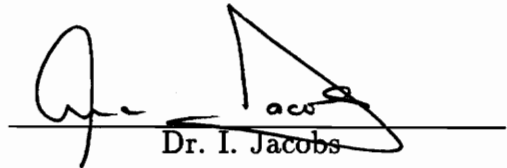


Dr. R. O. Claus, Chairman



---

Dr. T.-C. Poon



---

Dr. I. Jacobs

August, 1990

Blacksburg, Virginia

c.2

LD  
3655  
4855  
1990

T564

c.2

*[Faint, illegible handwritten text]*

**HIGH RESOLUTION OPTICAL TIME DOMAIN METHODS  
FOR MEASURING STRAIN**

by

**Daniel D. Thomas**

**Dr. R. O. Claus, Chairman**

**Electrical Engineering**

**(ABSTRACT)**

High resolution optical time domain methods applied to measuring strain in an optical fiber are discussed. The use of this optical time domain fiber sensor for measuring quasi-distributed strain along a cantilevered beam is experimentally demonstrated. This is accomplished by segmenting the sensor with air-gap sites, allowing reflections to be monitored. Physically looping these fiber segments many times over their interaction regions is shown to improve the sensitivity of the sensor. Also discussed are techniques to improve sensitivity by using a special tap-off coupler to recirculate optical pulses many times through the sensing region. Important in modeling these sensors is determining the photoelastic coefficient, which accounts for the photoelastic and Poisson effects on a strained fiber. The photoelastic coefficient is theoretically modeled using two methods involving waveguide and ray-optics theory. The results of these analyses are compared to experimentally determined values.

## ACKNOWLEDGEMENTS

I would like upmost to thank my family for all their love and support. My mother and father have given me the confidence to see that nothing is beyond my grasp. I wish to dedicate this work in memory of my niece, Kendra Laurel Houck, whose tremendous courage has made such an impact on my life.

I wish to sincerely thank my advisor, Dr. R. O. Claus, for his encouragement, aid, and guidance without which my stay here at Virginia Tech would not have been possible. I wish to thank Dr. I. Jacobs and Dr. T. C. Poon for serving on my graduate committee.

I express my sincere thanks to good friend Bernd Zimmermann for his guidance and patience during my research work. His invaluable innovation and experience saw me through many trouble spots. With his encouragement, I was able to overcome obstacles and complete this work. I wish to gratefully acknowledge Ashish Vengsarkar for his knowledge and never ending patience in much of the theoretical work accomplished here. Many thanks also go to my fellow graduate students and associates at the Fiber and Electro-Optics Research Center here at Virginia Tech who have made my graduate years so enjoyable.

## TABLE OF CONTENTS

1.0 INTRODUCTION .....	1
2.0 REVIEW OF OPTICAL TIME DOMAIN SYSTEMS .....	3
3.0 THEORY .....	8
3.1 Fiber Length Change From Time of Flight Measurements .....	8
3.1.1 Experimental Approach .....	9
3.1.2 Theoretical Approach .....	10
3.1.3 Ray-Optics Approach .....	14
3.2 Quasi-Distributed Strain Measurements .....	19
3.3 Resolution Improvements Using the Fiber Optic Reentrant Loop ....	24
4.0 EXPERIMENTS .....	30
4.1 Determination of the Strain-Optic Coefficient .....	30
4.2 Measurement of Quasi-Distributed Strain Along a Cantilever Beam ..	32
4.3 Fiber Optic Reentrant Loop Strain Measurements .....	40
5.0 PRACTICAL CONSIDERATIONS .....	44
6.0 CONCLUSION .....	46
APPENDIX A: Derivation of Strain Optic Coefficient .....	47
APPENDIX B: C Program .....	53
TABLE OF CONTENTS	

REFERENCES ..... 65

VITA ..... 67

## 1.0 INTRODUCTION

Optical fiber strain sensors have been investigated for more than a decade [1]. Optical fibers offer many advantages as sensors; optical fibers are manufactured of an all dielectric material, thus they have the properties of not conducting heat or electricity and also are immune to electromagnetic interference. Another advantage of using optical fibers as sensors is their low mass; their flexibility offers a wide variety of layout geometries for different applications. On a macroscopic scale, optical fiber strain sensors are one-dimensional and measure fiber length change, in fact the length change measured is a line integration of the strain over the sensor's path [2, 3]. This type of strain measurement provides a scalar output related to the distributed strain along the path.

It is sometimes of interest to obtain more information about the spatial distribution of strain along the fiber's length. Optical time domain methods offer the capability to make quasi-distributed strain measurements using a single sensor by measuring at discrete predetermined lengths along a segmented fiber. The output of this system would be an integer number of scalar outputs representing the line integrations of strain along each fiber segment. The applications for quasi-distributed sensing are numerous and include measuring strain on large space structures, bridges, dams, and pressure vessels [2].

Optical time domain systems measure the time of flight of an optical pulse to travel a particular optical fiber path [4]. A description of an optical time domain system and details on the one used for my analysis will be addressed in Chapter 2.

If an axial strain is applied to the sensing fiber, the fiber's length will change. This length change will change the optical pulse time of flight, which is measured. Along with the segmented fiber sensor, this thesis will also explore another optical time domain sensor, the fiber optic reentrant loop which uses a special fiber coupler to recirculate optical pulses through a sensing region many times. This improves the system's resolution for measuring the time of flight, thus increasing the sensitivity of the strain sensor. The calculation of length change for both the segmented and reentrant loop sensor will be discussed in the theoretical formulation of Chapter 3. Chapter 4 will explore the feasibility of these sensors experimentally. And finally, the practical considerations of the optical time domain strain sensors will be presented in Chapter 5.

## 2.0 REVIEW OF THE OPTICAL TIME DOMAIN SYSTEM

The schematic of a typical optical time domain system is shown in Figure 2.1. The system basically consists of a pulsed laser diode, an APD detector, a pulse delay generator, and a signal processor. The system that was utilized in this research effort is the Opto-Electronics TDR10/MF20 OTDR system. The laser diode produces a stable, nearly jitter free optical pulse that has a full width at half maximum of 160 ps. The optical pulses are launched into the near end of an optical fiber at a repetition rate of 33 kHz. The system can operate in either the transmissive or reflective mode. When operating in the transmissive mode, the terminating end of the fiber is connected to the photodetector. Reflective mode operation requires a fiber optic 2x2 coupler to be connected to the laser and photodetector. This allows pulses, that are reflected from a reflection site or the fiber end face, to be received by the photodetector. The adjustable time delay allows a pulse received in the reflective or transmissive mode to be searched for, located along the time axis, and displayed on an oscilloscope. The width of each division on the oscilloscope screen can be adjusted from 50 ps to 10 ns, allowing flexibility in locating a pulse's position. The time delay can accommodate a range of fiber lengths from 1 mm - 30 km [5, 6].

The Opto-Electronics system has many capabilities, including pulse loss and FWHM measurements. The capability exploited to make strain measurements possible is the precise locating of a received optical pulse in the time domain. The signal processor, within the optical time domain system, averages a received pulse many times to reduce random noise. Figure 2.2 is a photograph of a received

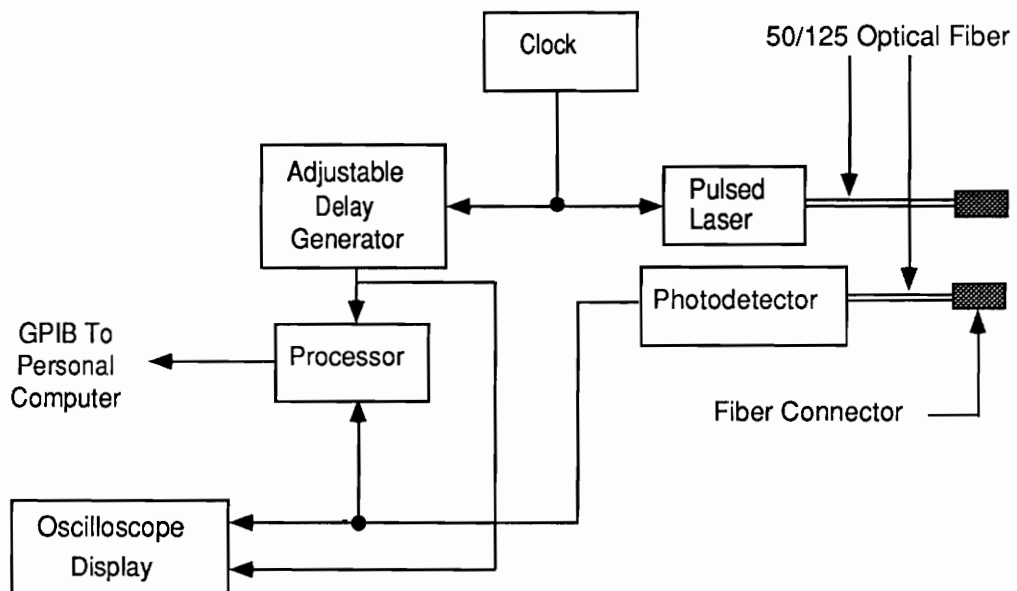


Figure 2.1. Block diagram of an optical time domain system.

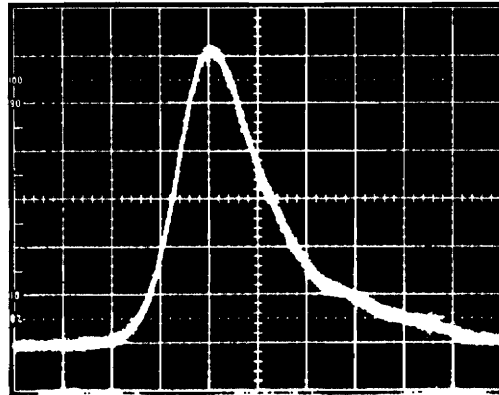


Figure 2.2. Reflected pulse averaged 512 times shown on an oscilloscope screen at 100 ps/division.

pulse that has been averaged 512 times, shown on an oscilloscope screen at 100 ps/division. The processor takes signals like this, fits a 16 point parabola to the peak of the averaged pulse, and determines the pulse's location in time to within +/- 1 ps, for no greater than a 100 ps/division time scale setting [5]. When monitoring a pulse to determine the change in length of a fiber, it is convenient to monitor the pulse location with respect to a reference pulse whose position does not fluctuate. When measuring the interval between two such pulses, the accuracy of the measurement is +/- 2 ps. At this point it is important to mention the limitations of the Opto-Electronics system. The dynamic range of received pulse amplitude, at a wavelength of 850 nm, is over 44 dB with a minimum voltage pulse amplitude of 4 mV. To obtain the maximum system resolution described, the pulse FWHM cannot exceed 650 ps, because the pulse will not fit on one oscilloscope screen width. If fiber dispersion results in a larger FWHM, then a setting higher than 100 ps/division can be used with a corresponding loss in pulse location resolution [5].

The dynamic range of fiber length change measurements using the Opto-Electronics system will now be addressed. Unlike the limited dynamic range of interferometric and modal domain measurements [1, 7, 8], the dynamic range of the optical time domain sensor is very large. Since measurements are not taken by observing interference patterns that oscillate every  $2\pi$  phase cycle, the time domain sensor can measure fiber length change linearly up until fiber breakage, which normally occurs for strains greater than 1.5 percent [9, 10]. The sensitivity of the sensor can be investigated by first examining the fiber length ( $l_f$ ) and optical pulse time of flight ( $t$ ) relationship for two-way optical time domain

reflectometry [5]

$$l_f = \frac{ct}{2n_1} , \quad (2.1)$$

where  $c$  is the velocity of light in vacuum and  $n_1$  is the group refractive index of the fiber core. The sensitivity is determined by substituting the accuracy of the measuring system, which is  $\pm 2$  ps, into equation (2.1). This results in an accuracy in determining fiber length change of approximately  $\pm 200$   $\mu\text{m}$ . Improving this limitation has been the motivation for the novel fiber sensor configurations discussed in this thesis.

## 3.0 THEORY

### 3.1 Fiber Length Change From Time of Flight Measurements

When axial strain is applied to the sensing fiber, the length of the fiber changes. This length change can be determined by using optical time domain methods to measure the change in the time of flight of an optical pulse that has traveled through the fiber. This can be shown by first considering the length of an optical fiber,  $l_f$ , given by

$$l_f = v_g t, \quad (3.1)$$

where  $t$  is the time for an optical pulse to travel one way down the fiber and  $v_g$  is the group velocity of an optical pulse traveling along the fiber. It is important to correlate variations in pulse arrival times to changes in fiber length. Important to this correlation are the photoelastic effect, which involves changes in the core and cladding refractive indices, and the Poisson effect, which describes the change in core diameter. The contribution the photoelastic effect and Poisson's effect have on the optical pulse temporal shift is given by the photoelastic coefficient. There are two approaches to evaluate the photoelastic coefficient. The experimental approach uses empirical data to calculate this effect, and the theoretical approach examines how the photoelastic coefficient varies with modal content of the electromagnetic field propagating through of the fiber. The two approaches will now be described in detail. The experimental approach is used in the analysis of the sensors examined in this thesis; however, investigating the theoretical approach gives some qualitative insight into what is actually happening when a fiber is axially strained.

### 3.1.1 Experimental Approach

The experimental approach to determine the photoelastic coefficient makes the assumption that the group velocity is the same for all propagating modes and can be approximated by the speed of light in vacuum,  $c$ , divided by the group refractive index of the fiber core,  $n_1$ . With this assumption, both sides of equation (3.1) are differentiated yielding [11]

$$dl_f = \frac{c}{n_1} dt - \frac{ct}{n_1^2} dn. \quad (3.2)$$

Substituting  $l_f$  of equation (3.1) into equation (3.2) results in

$$dl_f = \frac{c}{n_1} dt - l_f \frac{dn_1}{n_1}. \quad (3.3)$$

As a consequence of the fiber length change, the measured pulse arrival time shifts and the core index of refraction changes due to the photoelastic effect. The core index of refraction versus axial fiber strain relationship is assumed to be linear where the slope of this line will be denoted as the photoelastic coefficient,  $a$ . This relationship is expressed as [11]

$$\frac{dn_1}{n_1} = a\epsilon_f = a \frac{dl_f}{l_f}, \quad (3.4)$$

where  $\epsilon_f$  is the axial strain applied to the fiber. Substituting equation (3.4) into equation (3.3) yields

$$\Delta l_f = \frac{c\Delta t}{n_1} \left( \frac{1}{1+a} \right), \quad (3.5)$$

where  $dl_f$  and  $dt$  are approximated by  $\Delta l_f$  and  $\Delta t$ , respectively. It is interesting

to note from equation (3.5) that the change in length of the fiber is evaluated without knowledge of the fiber sensor's length. However, if the interaction length,  $l_f$ , of the sensing fiber is known, the axial strain,  $\epsilon_f$ , on the fiber section can be resolved using the relation

$$\epsilon_f = \frac{\Delta l_f}{l_f}. \quad (3.6)$$

It is often convenient to measure  $\Delta t$  using optical time domain reflectometry to monitor the Fresnel reflection that occurs from the cleaved endface of the fiber sensor. When the optical time domain system is operated in this fashion, the launched optical pulse travels twice the distance of the optical fiber. Figure 3.1 shows an example of the sensor adhered to a flexible structure. A given change in fiber length will change the pulse arrival time by twice as much as if the terminating end of the sensor was placed at the system's photodetector. This relation can be expressed by modifying equation (3.5) yielding [11]

$$\Delta l_f = \frac{c\Delta t}{2n_1} \frac{1}{(1 + a)}. \quad (3.7)$$

### 3.1.2 Theoretical Approach

From equation (3.5), measuring  $\Delta t$  and knowing the photoelastic coefficient,  $a$ , we can deduce the change in fiber length. Accurate results have been obtained, with this formulation, for graded-index fibers which will be shown in Chapter 4. However, it will also be shown that step-index multimode fibers cannot be modeled accurately with the previous analysis. Since the modal content of step-index multimode fibers is more sensitive to external perturbations than graded-

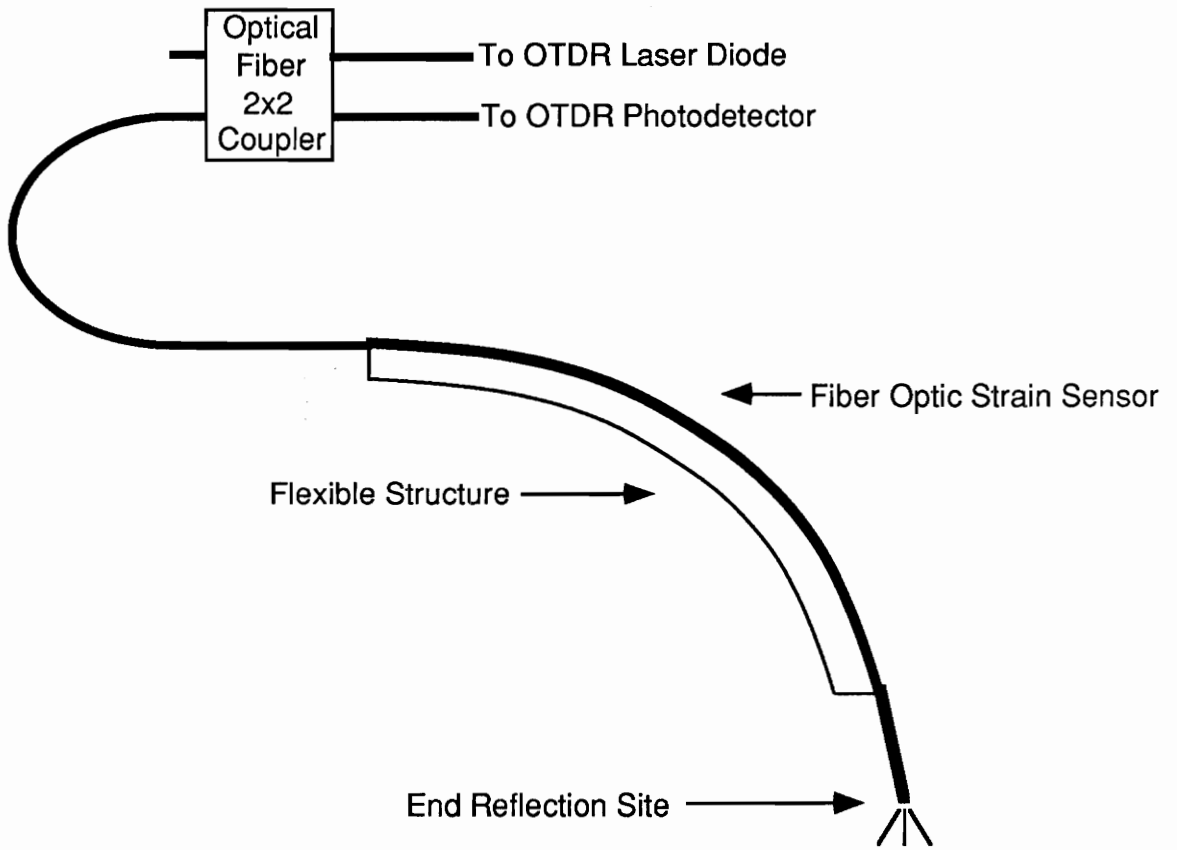


Figure 3.1. Optical time domain strain sensor adhered to a flexible structure.

index fibers, this has led to the hypothesis that the photoelastic coefficient is dependent on the modal content of the fiber. The approach has therefore been modified to explore this dependency. Determining the coefficient using the theoretical approach takes into consideration that, when a fiber is axially strained the group velocity changes differently for each optical mode traveling along the fiber. This relationship can be expressed by differentiating equation (3.1) yielding

$$\Delta l_f = v_g \Delta t + t \Delta v_g, \quad (3.8)$$

where  $dl_f$ ,  $dt$ , and  $dv_g$  are approximated by  $\Delta l_f$ ,  $\Delta t$ , and  $\Delta v_g$ , respectively. Substituting equation (3.1) into equation (3.8) gives

$$\Delta l_f = v_g \Delta t + \frac{l_f}{v_g} \Delta v_g. \quad (3.9)$$

The change in fiber length results in a measured optical pulse arrival time shift, and, due to the physics of the problem, a change in group velocity for each propagating mode. We should also consider that both  $v_g$  and  $\Delta v_g$  are modally dependent parameters, thus it is possible to calculate different length changes with the same  $\Delta t$  given different modal conditions. This analysis is expressed in detail in Appendix A. To obtain insight into the magnitude of this effect,  $v_g$  and  $\Delta v_g$  are expressed in terms of the tabulated waveguide quantity,  $d(bV)/dV$ , and the normalized propagation constant,  $b$ . The group velocity given in equation (A.9) is

$$v_g = \frac{d\omega}{d\beta} = \frac{2c \sqrt{b(n_1^2 - n_2^2) + n_2^2}}{(n_1^2 - n_2^2) \left(b + \frac{d(bV)}{dV}\right) + 2n_2^2}. \quad (3.10)$$

The change in group velocity is represented by the differential summation of the Poisson effect and the photoelastic effect, which are the changes in the core radius,  $\Delta r$ , and the core and cladding refractive indices,  $\Delta n_1$  and  $\Delta n_2$ , respectively. This is expressed in equation (A.2) as

$$\Delta v_g = \frac{\partial v_g}{\partial r} \Delta r + \frac{\partial v_g}{\partial n_1} \Delta n_1 + \frac{\partial v_g}{\partial n_2} \Delta n_2. \quad (3.11)$$

Substituting equations (3.10) and (3.11) into equation (3.9) is given by equation (A.17) as

$$\Delta l_f = \frac{\Delta t v_g}{1 + \frac{1}{v_g} \left[ \mu r \frac{\partial v_g}{\partial r} + \frac{1}{2} n_1^3 P \frac{\partial v_g}{\partial n_1} + \frac{1}{2} n_2^3 P \frac{\partial v_g}{\partial n_2} \right]}. \quad (3.12)$$

The  $\Delta l_f$  to  $\Delta t$  relationship of equation (3.12) is very similar to that of equation (3.5). The second term in the denominator represents the photoelastic coefficient, where  $\mu$  is Poisson's ratio and  $P$  is the photoelastic effect as defined in Appendix A.

It is of interest to examine how the photoelastic coefficient term of equation (3.12) varies with modal content. For this analysis, a 200/240  $\mu\text{m}$  in diameter step-index fiber is considered. The core radius,  $r$ , is 100  $\mu\text{m}$ , core and cladding refractive indices,  $n_1$  and  $n_2$ , are 1.458 and 1.45, respectively, and the wavelength of the laser is 850 nm. For typical silica fibers, Poisson's ratio,  $\mu$ , and the strain-

optic coefficients,  $p_{11}$  and  $p_{12}$ , are 0.16, 0.113, and 0.252, respectively [12].

Figure 3.2 shows a plot of the photoelastic coefficient,  $a$ , as calculated from the second term in the denominator of equation (3.12) as a function of the normalized propagation constant,  $b$ . The range of  $b$  was chosen to approach 1 and the Bessel order,  $l$ , to be 0; this describes a small range of low order propagating modes. The graph shows a variation in the photoelastic coefficient for this range of propagating modes. The objective is to examine the behavior of the coefficient from high order to low order modes. It is evident that this model is not correct due to the behavior of the function over all possible values of  $b$ , which ranges from 0 to 1. The photoelastic coefficient actually becomes positive, which is unphysical. This waveguide model could be more thoroughly analyzed with high order  $b$  versus  $V$  curves, which might allow examination of the photoelastic coefficient variation for higher order modes.

### 3.1.3 Ray-Optics Approach

The analysis just described was a systematic approach of determining the photoelastic coefficient using waveguide theory. The approach was found to have limited results, so a more simplified theoretical approach will now be developed using ray-optics theory. This approach examines the change in the photoelastic coefficient with respect to which electromagnetic mode is propagating. A geometrical model for the fiber that describes the propagation of the different order modes is shown in Figure 3.3. We consider the propagation of a mode at an angle,  $\alpha$ , to the longitudinal axis of the fiber. Different order modes will propagate at different  $\alpha$ 's according to the ray-optic approach. Although only

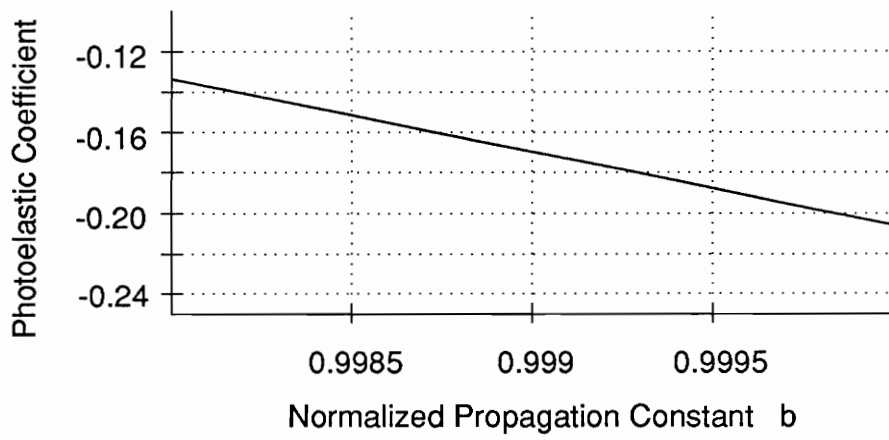


Figure 3.2. Variation of photoelastic coefficient using waveguide theory approach.

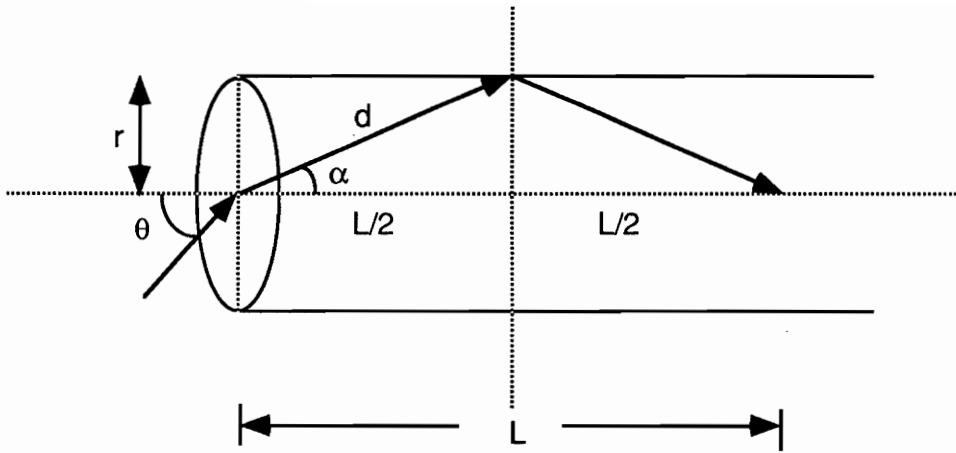


Figure 3.3. Fiber core diagram for ray-optics approach.

those  $\alpha$ 's that satisfy the phase-matching criterion after one reflection at the core-cladding interface will propagate as guided modes, equations will be derived that are applicable for all  $\alpha$ 's.

The analysis begins by defining the distance,  $d$ , traveled by the optical mode as a function of launch angle,  $\alpha$ , as

$$d = \frac{L}{2} \sec\alpha, \quad (3.13)$$

where  $L$  is the length of fiber required for the ray to return to the central axis. The time,  $t$ , required for the ray to travel this length of fiber is given by

$$t = \frac{2d}{v_g} = \frac{n_1 L \sec\alpha}{c}. \quad (3.14)$$

The relation of the observed pulse shift,  $\Delta t$ , for a fiber length change,  $\Delta L$ , can again be shown as the summation of three effects; these are the change in fiber length, the photoelastic effect, and the Poisson effect. These three effects can be expressed mathematically by differentiating both sides of equation (3.14) yielding

$$\Delta t = \frac{1}{c} [L \sec\alpha \Delta n_1 + n_1 \sec\alpha \Delta L + n_1 L \Delta(\sec\alpha)]. \quad (3.15)$$

The three differentials on the right side of equation (3.15) will now be defined individually. We first examine  $\Delta(\sec\alpha)$ , given by

$$\Delta(\sec\alpha) = \Delta\left[\sqrt{1 + \frac{4r^2}{L^2}}\right] = \frac{1}{2}\left(1 + \frac{4r^2}{L^2}\right)^{-\frac{1}{2}} \left[\frac{8r}{L^2}\Delta r - \frac{8r^2}{L^3}\Delta L\right], \quad (3.16)$$

where  $\Delta(\sec\alpha)$  is equal to the sum of the partials with respect to  $r$  and  $L$ . The change in the fiber core refractive index and the change in core radius will be defined as in Appendix A as

$$\Delta n_1 = -\frac{1}{2} \frac{\Delta L}{L} n_1^3 [(1 - \mu)p_{12} - \mu p_{11}] = -\frac{1}{2} \frac{\Delta L}{L} P, \text{ and} \quad (3.17)$$

$$\Delta r = -r\mu \frac{\Delta L}{L}, \quad (3.18)$$

respectively. Substituting equations (3.16), (3.17), and (3.18) back into equation (3.15) and solving for the change in length,  $\Delta L$ , yields

$$\Delta L = \frac{c\Delta t}{n_1} \frac{1}{\sec\alpha - \frac{Pn_1^2 \sec\alpha}{2} - \frac{(1 + \mu)(\sec^2\alpha - 1)}{\sec\alpha}}. \quad (3.19)$$

Comparing equation (3.19) to equation (3.5), the photoelastic coefficient,  $a$ , can be expressed as

$$a = \sec\alpha - \frac{Pn_1^2 \sec\alpha}{2} - \frac{(1 + \mu)(\sec\alpha - 1)}{\sec\alpha} - 1. \quad (3.20)$$

It is of interest to plot the above equation over the range of all possible  $\alpha$ 's, which is defined by the fiber's numerical aperture. The fiber to be analyzed is the 200/240 step-index fiber. The fiber's manufacturer, Polymicro Technologies Incorporated, claims that at a wavelength of 850 nm, the numerical aperture to be 0.22; this gives a range for  $\alpha$  of 0 degrees for the first mode, which travels

straight down the fiber's central axis, to 9 degrees for the highest order mode. However, manufacturers typically measure the numerical aperture for step-index fibers for lengths over a kilometer. At this length, many of the higher order modes have been lost. Since the sensors for this research effort are usually less than twenty meters, a more accurate numerical aperture is 0.35 producing a range for  $\alpha$  of 0 to 14 degrees. The values for Poisson's coefficient and the strain-optic coefficients will be the same as used in the waveguide approach. Using these values, Figure 3.4 shows a graph of the photoelastic coefficient against the launch angle,  $\alpha$ . The variation of the coefficient is evident as higher order modes are excited. The ray-optics approach proved to be very useful for a qualitative look as to why large-core step index fibers give a large variation in the photoelastic coefficient. This approach predicts a variation in the coefficient to be approximately from -0.2 to -0.26.

### **3.2 Quasi-Distributed Strain Measurements**

The quasi-distributed strain sensor, in which the optical time domain system is operated in the reflective mode, is a fiber that has been segmented with each segment separated by a partially reflecting Fresnel site. The Fresnel reflection site described in [11] was found to be rugged due to the metallic cylinder encapsulating it. This design is especially useful for applications such as embedding the sensor in a composite material where the site would have to be strain relieved, so the gap distance would remain constant. However, the air gap splice proved to be bulky, so a smaller reflection site was designed for this research effort. The design chosen is shown in Figure 3.5. The miniaturized

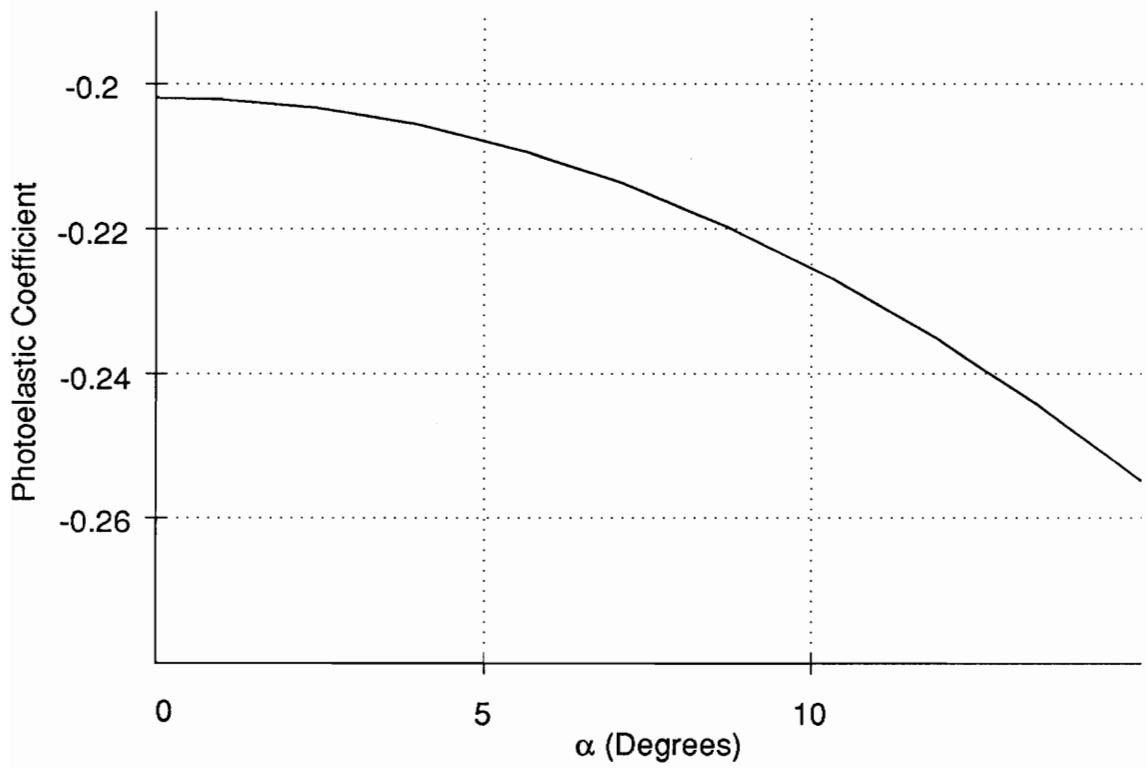


Figure 3.4. Variation of photoelastic coefficient with launch angle using ray-optics approach.

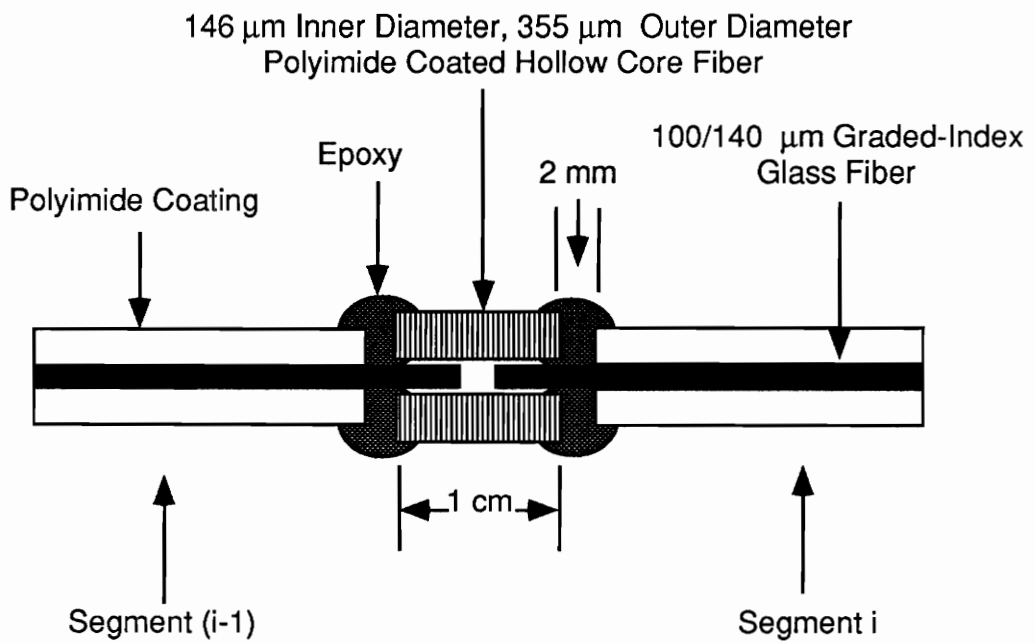


Figure 3.5. Miniaturized Fresnel reflection site.

Fresnel reflection site is less rugged, but is simpler to implement and could be useful in certain applications where size is critical and the site does not have to be strain relieved. The transmission loss through the site, which is obtained for a gap distance from 5-50  $\mu\text{m}$ , is 0.5 dB. With this loss, a conservative estimate for the number of segments in a single sensor is 20. This number is obtained by considering the amplitude of the pulse that has reflected from the terminating end of the sensor and traveled back through the reflection sites. An illustrative example of the quasi-distributed sensor is shown in Figure 3.6. The optical time domain system launches pulses into the segmented sensor of which a portion of the pulse power is reflected at each Fresnel reflection site back to the photodetector while most of the pulse's power is transmitted through the site to the next. When axial stress is applied to this sensor, each segment length in general will change by a different amount. If length changes smaller than the resolution of the system are to be measured, it is useful to pass a segment length back and forth over the sensing region many times, increasing the interaction length of the sensor. The optical pulse will be shifted by each fiber pass over the region of interest thus improving the resolution of the sensing segment. The number of fiber passes is referred to as the resolution improvement factor. The length change in each segment can be obtained by measuring the change in pulse arrival times at the photodetector. Using the experimental approach approximation of the photoelastic coefficient, the relationship can be obtained by first considering the expression for the fiber length,  $l_{f,i}$ , of the  $i^{\text{th}}$  segment [11] as

$$l_{f,i} = \left[ \frac{1}{2j_i} \right] \left[ \frac{c}{v_1} \right] (t_i - t_{i-1}), \quad (3.21)$$

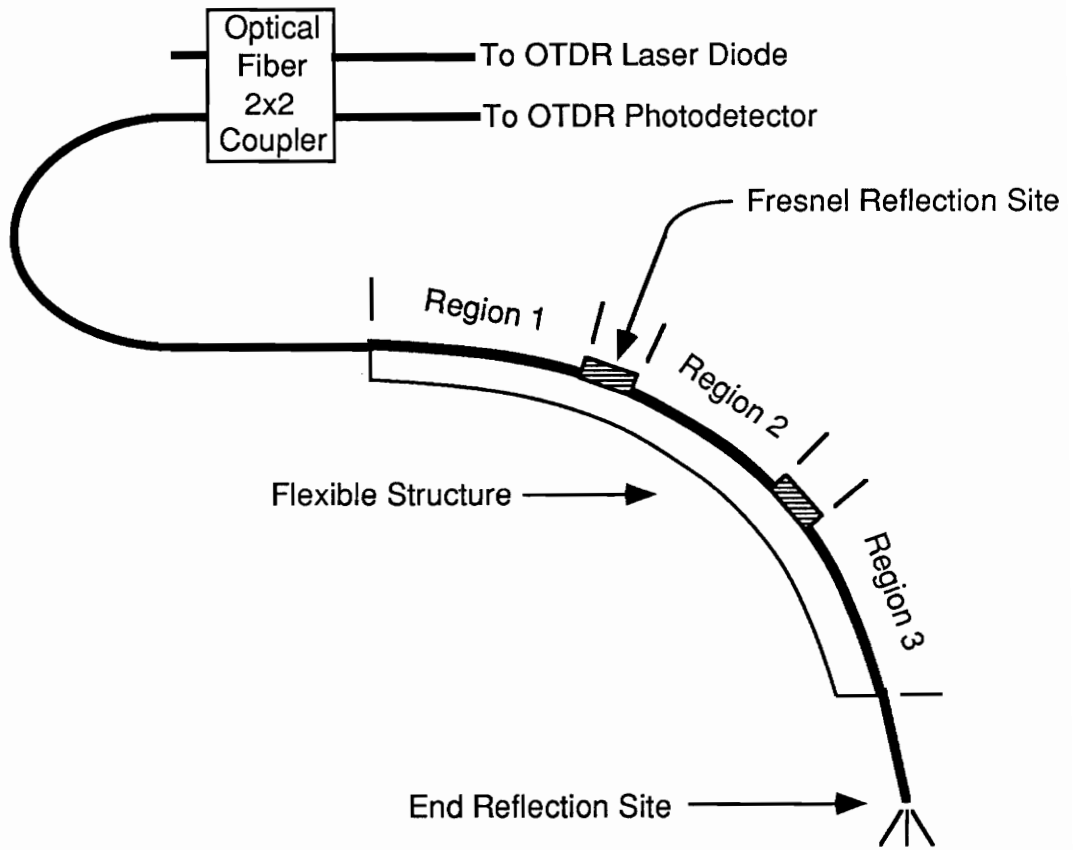


Figure 3.6. Quasi-distributed strain sensor adhered to a flexible structure.

where  $j_i$  is the resolution improvement factor for segment  $i$ ,  $t_i$  is the time for the optical pulse to travel to the far end Fresnel reflection site of segment  $i$  and back, and  $t_{i-1}$  is the time for the optical pulse to travel to the near end site of segment  $i$  and back. Differentiating both sides of equation (3.21) yields

$$dl_{f,i} = \left[ \frac{c}{2j_i n_1} \right] [(dt_i - dt_{i-1}) - \frac{dn}{n} (t_i - t_{i-1})]. \quad (3.22)$$

Substituting equation (3.21) into equation (3.22) yields

$$dl_{f,i} = \frac{c}{2n_1 j_i} (dt_i - dt_{i-1}) - \frac{dn_1}{n_1} l_{f,i}. \quad (3.23)$$

The final result correlating the arrival times of the reflected pulses is obtained by substituting equation (3.4) into equation (3.23) to obtain

$$\Delta l_{f,i} = \frac{c}{2n_1 j_i} (\Delta t_i - \Delta t_{i-1}) \frac{1}{(1 + a)}, \quad (3.24)$$

where  $dl_{f,i}$ ,  $dt_i$ , and  $dt_{i-1}$  are approximated by  $\Delta l_{f,i}$ ,  $\Delta t_i$ , and  $\Delta t_{i-1}$ , respectively.

### 3.3 Resolution Improvements Using The Fiber Optic Reentrant Loop

It is recognized that certain applications of the optical time domain sensor would require large resolution improvement factors. Obtaining this improvement by physically passing the fiber back and forth over the sensing region can prove to be bulky and inefficient. To better this method of resolution improvement, a pulse recirculation scheme was implemented using fiber optic reentrant loops [13-15].

This method would increase the interaction length of the strain sensor by the number of times the pulse propagates around the loop.

Figure 3.7 shows an example of the reentrant loop strain sensor adhered to a flexible structure. The important component of the reentrant loop is the tap-off coupler. This coupler is designed from two large-core, step-index fibers, which are 50/125  $\mu\text{m}$  and 200/240  $\mu\text{m}$  in diameter. The optical pulses enter the tap-off coupler through the 50/125  $\mu\text{m}$  fiber after which approximately 50% of the power is coupled onto the 200/240  $\mu\text{m}$  fiber loop. Once the pulse is in the loop, about 95% of the power remains recirculating while the remaining pulse power is coupled to the photodetector of the optical time domain system. The fibers should have step-index profiles such that the tap-off ratios are 95% - 5%, with the higher order modes being stripped off at every recirculation. Figure 3.8 is a photograph of the received optical pulses from the reentrant loop on an oscilloscope screen at 10 ns/division. The pulse on the far left is pulse 0 and was coupled straight onto the 50/125  $\mu\text{m}$  return fiber without passing through the loop. The next pulse from the left of the oscilloscope screen, which is pulse 1, has circulated once around the loop, and each subsequent pulse has circulated an additional time.

The optical pulses are subjected to two effects as they continue to recirculate around the fiber loop. The first effect is power loss. In Figure 3.8, the exponential loss of pulse amplitude is evident. The pulse-to-pulse loss can range from 0.36 dB to 0.7 dB as the manufacturing of the tap-off couplers varies. Although the splitting ratio is the dominant effect in power loss, it was observed that the power loss became less for larger recirculation numbers. This effect was

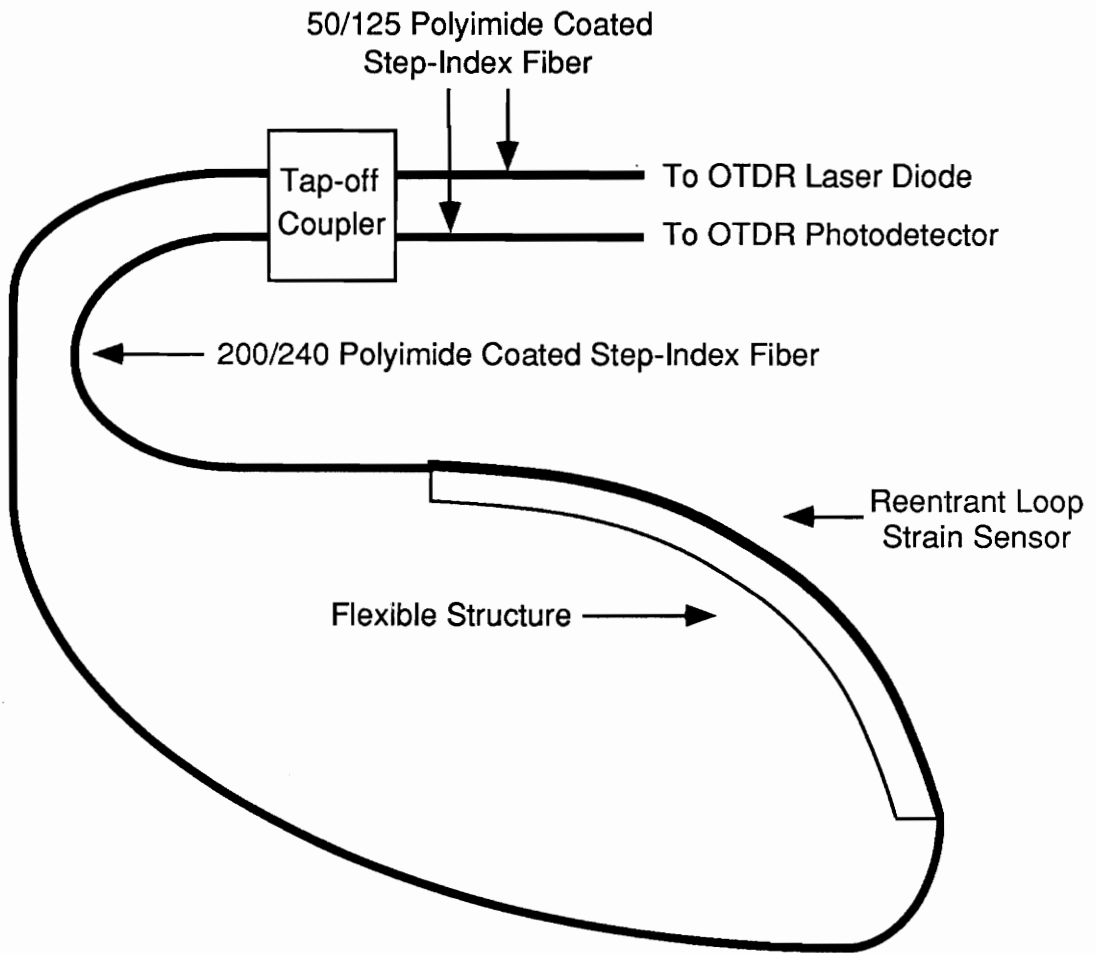


Figure 3.7. Reentrant loop strain sensor adhered to a flexible structure.

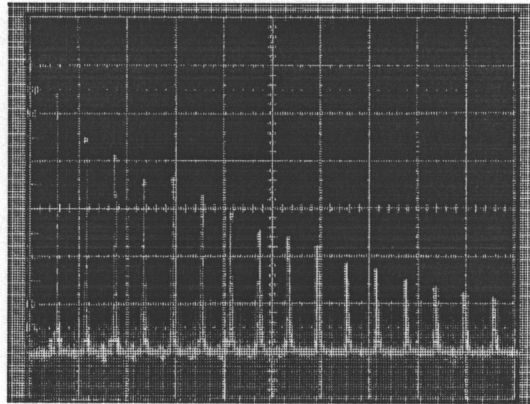


Figure 3.8. Typical reentrant loop received optical pulse signature shown on an oscilloscope screen at 10 ns/division.

attributed to a change in modal composition of the field in the large-core 200/240  $\mu\text{m}$  step-index fiber. Power in the higher order modes is being lost with each pass through the tap-off coupler. A modal equilibrium is therefore attained with sufficient recirculation. The second effect the pulses experience is dispersion. Dispersion is relatively high, on the order of 10 ps/m, in the 200/240  $\mu\text{m}$  step-index fiber. The dispersion and power loss represent the limitations on the practical number of pulse recirculations available to the system. The limitations of the optical time domain system were presented in Chapter 2.

The correlation of received optical pulse shift to change in the reentrant loop length will now be developed. Once again, the experimental approach approximation will be used to obtain the photoelastic coefficient. The expression for the length,  $l_{f,i}$ , of a single pass of the fiber over the interaction region for the  $i^{\text{th}}$  recirculation is given by

$$l_{f,i} = \frac{c}{ij n_1} t_i, \quad (3.25)$$

where  $j$  is the number of physical passes over the interaction region by the fiber sensor, and  $t_i$  is the time for the optical pulse to travel through the sensor  $i$  times. Differentiating both sides of equation (3.25) yields

$$dl_{f,i} = \frac{c}{ij n_1} \left[ dt_i - \frac{dn_1}{n_1} l_{f,i} \right]. \quad (3.26)$$

A relation to the shift in pulses recirculating  $i$  times to length change of a single fiber pass is obtained by substituting equation (3.4) into equation (3.26), which gives

$$\Delta l_{f,i} = \frac{c}{ij n_1} \Delta t_i \frac{1}{(1+a)}, \quad (3.27)$$

where  $dl_{f,i}$  and  $dt_i$  are approximated by  $\Delta l_{f,i}$  and  $\Delta t_i$ , respectively. The resolution improvement factor of this strain sensor is  $ij$ , which is the multiplication of the number of loop recirculations and the number of physical sensor passes over the interaction region.

## 4.0 EXPERIMENTS

### 4.1 Determination of the Photoelastic Coefficient

In order to evaluate the practicality of the optical time domain strain sensor, the photoelastic coefficient of 100/140  $\mu\text{m}$  in diameter polyimide coated graded-index fiber had to be determined. Polyimide coated fibers were chosen because of the strong bonding of the coating to the fiber cladding eliminating any slippage or pistonning between coating and glass. The concept behind determining the photoelastic coefficient is to change the fiber's length by a known amount and measure the corresponding change in pulse arrival time. We begin with a description of the experimental setup used to evaluate this coefficient.

The experimental setup is shown in Figure 4.1. A length of optical fiber is secured at two places with one end fixed and the other attached to a micrometer translation stage. A clamp could not be used to hold the fiber as this would flaw the fiber's surface or cause extreme side loading. To secure both ends of the fiber, they were potted in "boats" of Bipax epoxy made by TRA-CON, Inc. Once the epoxy hardened, the boats were clamped in place so that lateral stress on the fiber was minimized. The fiber end face was then cleaved so a strong Fresnel reflection occurred.

The starting position of the micrometer for this experiment made the fiber taut, so no slack was in the fiber. Using the optical time domain system, measurements of the change in pulse time of flight were then taken at each increment of fiber

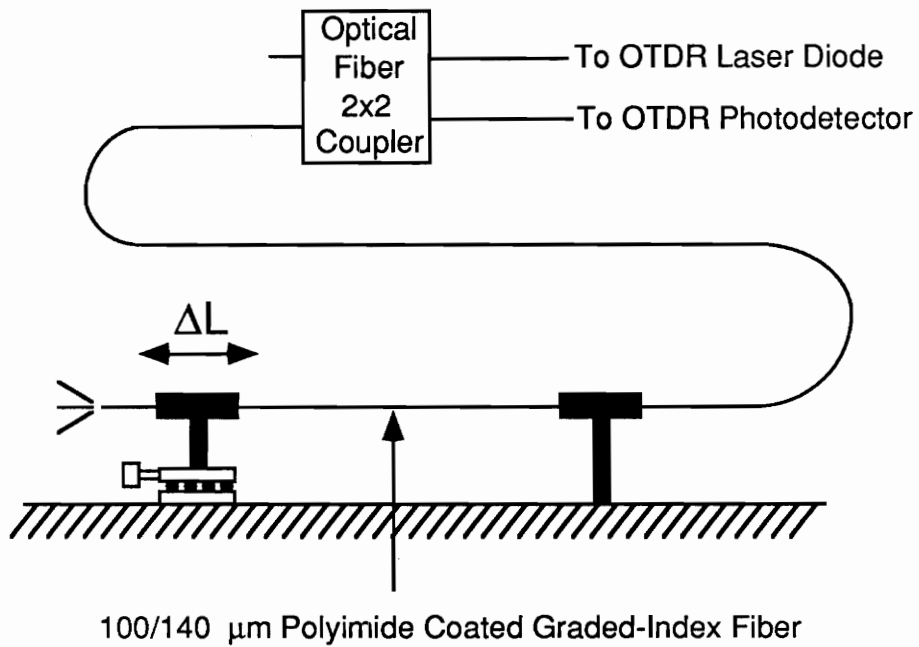


Figure 4.1. Experimental setup for determining the photoelastic coefficient

elongation. The fiber was elongated in increments of 250  $\mu\text{m}$  up to 3000  $\mu\text{m}$ . The reference pulse used here was the free floating end of the 2x2 coupler. To reduce the error in pulse position determination, these measurements and all subsequent experimental data were taken with the aid of a personal computer driven by a computer program written to interface the optical time domain processor via a general purpose interface bus (GPIB) port. The program was developed in the C language and averages a user specified number of pulse position measurements and monitors any processor instability, which seems to be specific to the particular optical time domain unit used for this research. Appendix B contains a listing of this program. For the experiments performed in this research effort, it was found to be optimum to use five pulse position averages with each position determined through 512 sweeps of the received pulse from the detector. This proved to be the most reliable method for reducing noise in the system.

This experiment was performed ten times to obtain the variation in determining the photoelastic coefficient. One of the data sets obtained is shown in Figure 4.2, which is a plot of fiber elongation against measured pulse shift. Equation (3.7) was used to back calculate the photoelastic coefficient,  $a$ , for each data set. The average value was found to be -0.200 with a standard deviation of 0.028.

## **4.2 Measurement of Quasi-Distributed Strain Along a Cantilever Beam**

The following experiment was designed to demonstrate the feasibility of the segmented optical time domain sensor for measuring strain on a quasi-distributed basis. The setup involved adhering the sensor to a flexible structure and, as the

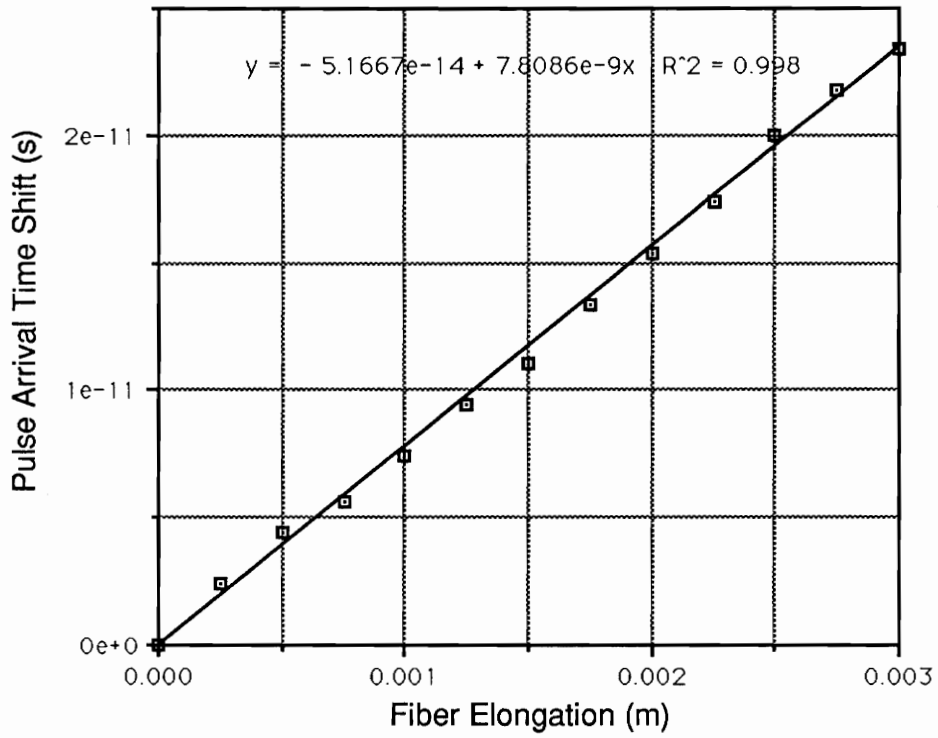


Figure 4.2. Example data set from photoelastic coefficient experiment using 100/140  $\mu\text{m}$  graded-index fiber.

structure's shape was altered, the sensor's length would be changed. The flexible structure used was an aluminum cantilever beam 1.1 m long, 9 cm wide, and 0.248 cm thick. The cantilever beam was chosen because a large amount of surface deformation can be introduced and the beam is easily modeled. The optical fiber used for this experiment was polyimide coated 100/140  $\mu\text{m}$  graded-index. A description of the quasi-distributed strain sensing experiment will now follow.

A diagram of the experimental setup is shown in Figure 4.3. A coordinate system is assigned such that  $x=0$  is at the tip of the cantilever beam and  $y=0$  represents the perpendicular tip resting position. Sensor 1 is adhered to the beam to measure the strain along  $x=1$  m to  $x=0.8$  m with fifteen fiber passes over the region. Sensor 2 will measure strain along  $x=0.73$  m to  $x=0.53$  m region with seventeen fiber passes and sensor 3 will measure strain along the region  $x=0.46$  m to  $x=0.26$  m with twenty-five fiber passes. The increasing number of fiber passes is intended to improve sensor resolution as strain decreases toward the tip. The sensors were adhered using Duralco 4525 high temperature epoxy made by Cotronics Corporation. This epoxy was chosen because its slow curing time made handling and application desirable. The epoxy also showed no measurable hysteresis effect.

The experiment was performed by deflecting the beam tip in increments and measuring the change in arrival times of the pulses reflected from the two Fresnel reflection sites and the pulse reflected from the glass-air interface at the terminating end of sensor 3. The reference pulse used was the free floating end of

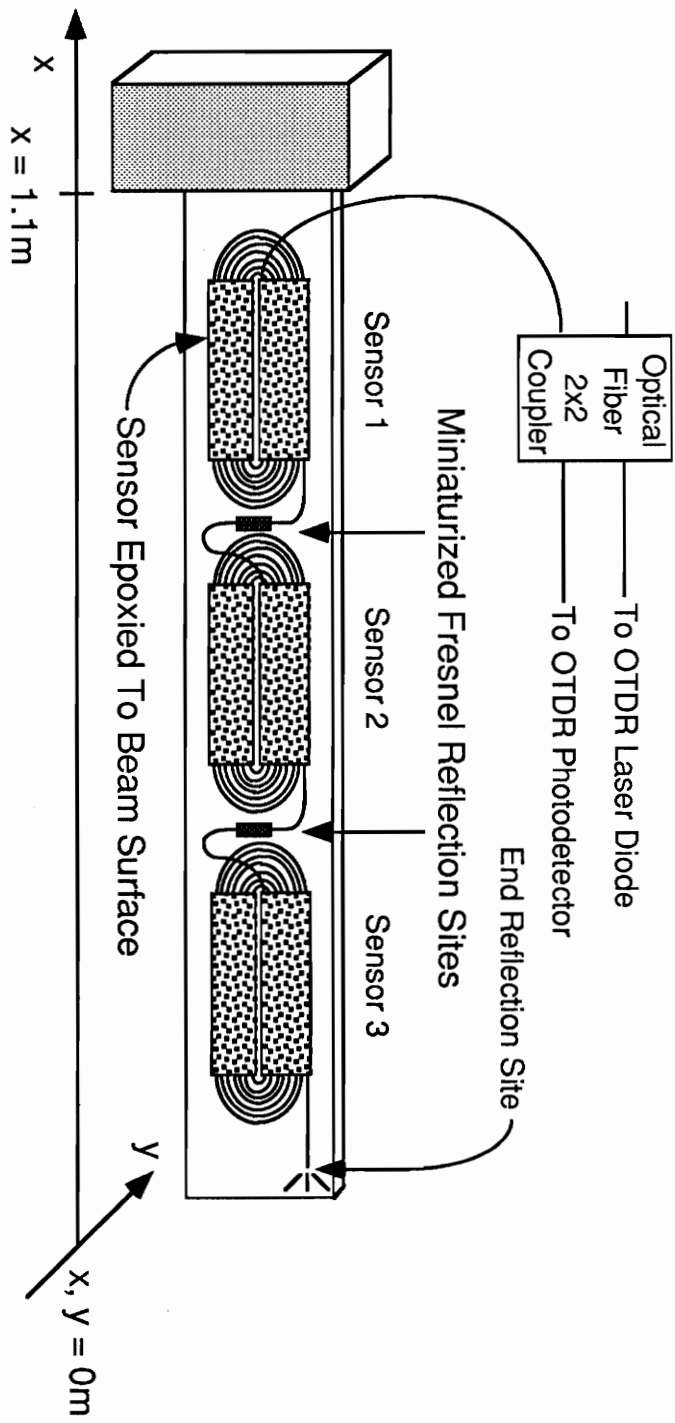


Figure 4.3. Static quasi-distributed strain sensing experimental setup.

the 2x2 coupler. Using equation (3.24), the unit change in fiber length for each sensor was calculated. For this calculation, the photoelastic coefficient used is the empirically determined value found in section 4.1 and the resolution improvement factors for sensor 1, 2, and 3 is fifteen, seventeen, and twenty-five, respectively. These results are compared with predicted values of cantilever beam surface deformation. To obtain these predicted values, we will first look at the relation of strain,  $\epsilon(x)$ , at any point  $x$  on a cantilever beam due to tip displacement,  $y$ , which is given by [16],

$$\epsilon(x) = \frac{3yx}{L^3} \frac{T}{2}, \quad (4.1)$$

where  $L$  is the length of the cantilever beam and  $T$  is the beam's thickness. Surface deformation,  $\Delta L_{1,2}$ , can be found between two points,  $x_1$  and  $x_2$ , by integrating both sides of equation (4.1)

$$\Delta L_{1,2} = \int_{x_1}^{x_2} \epsilon(x) dx = \frac{3yT}{4L^3} \left[ x^2 \right]_{x_1}^{x_2}. \quad (4.2)$$

Using equation (4.2), the predicted surface deformation lines for the three sensing regions are plotted against calculated fiber length change from the three measured data sets. The plots for sensors 1, 2, and 3 are shown in Figures 4.4, 4.5, and 4.6 respectively. Each plot gives a comparison of the predicted line equation to the linear regression of the data set. Sensor 1 produces the best results as this region was subjected to the largest strain. This good correlation also demonstrated the ability of the optical time domain sensor to detect compressive or negative strain.

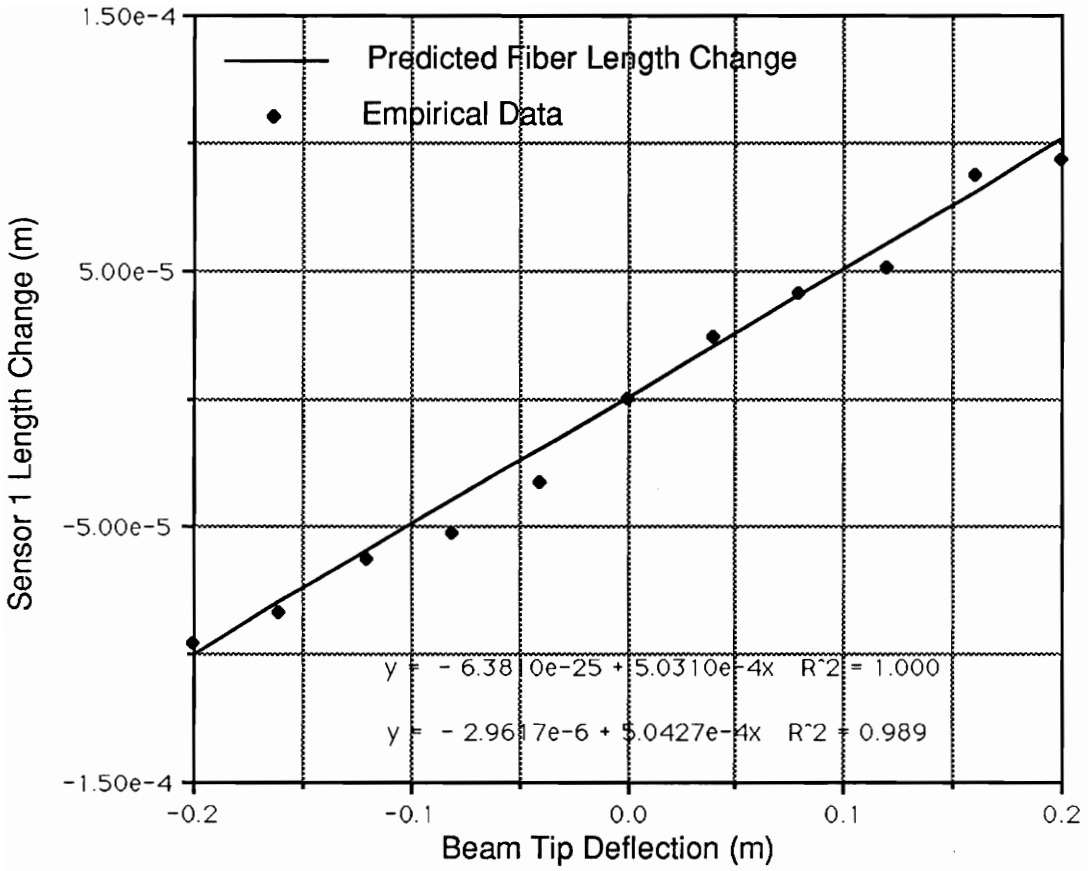


Figure 4.4. Sensor 1 measured and predicted fiber length change.

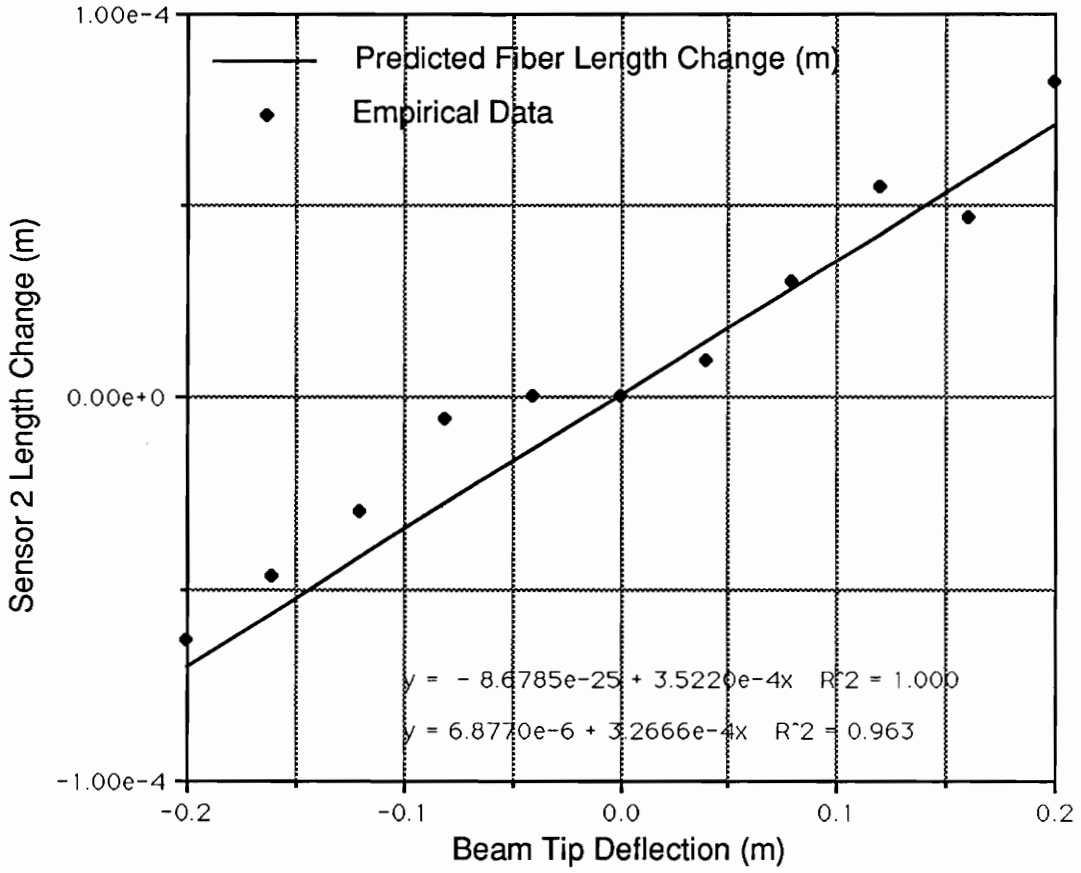


Figure 4.5. Sensor 2 measured and predicted fiber length change.

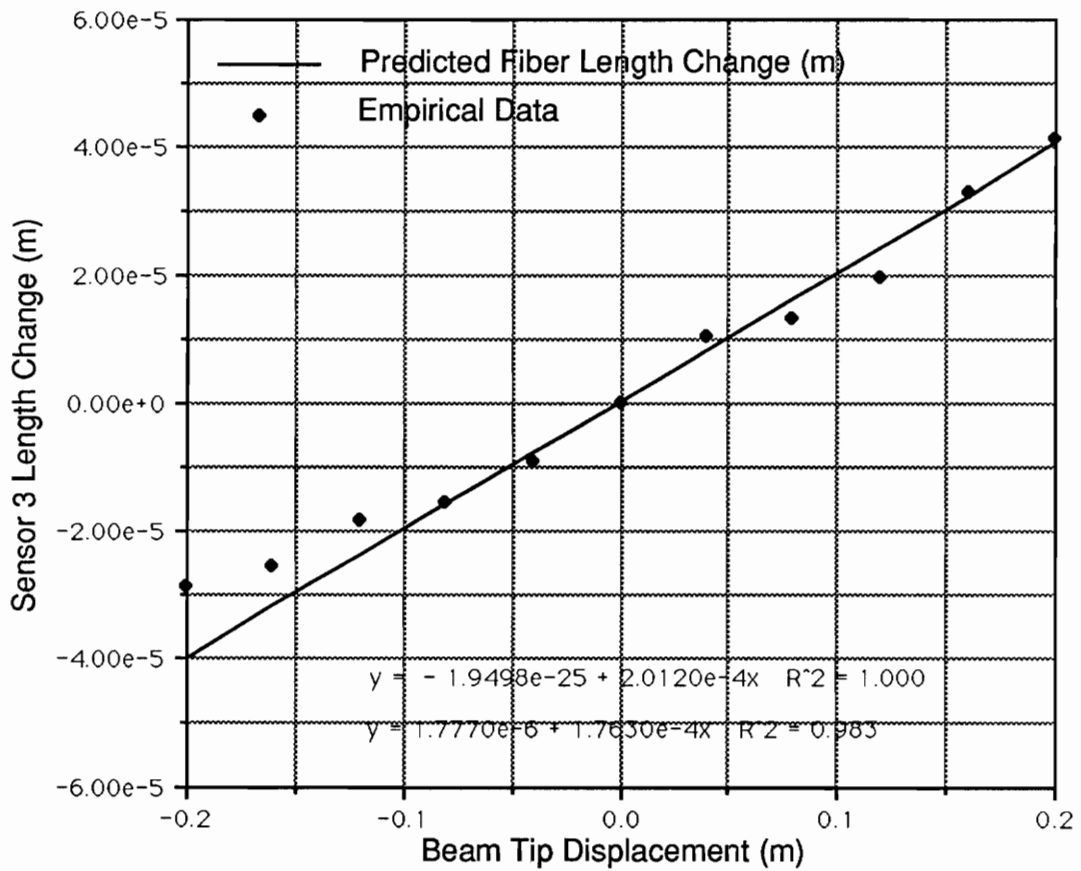


Figure 4.6. Sensor 3 measured and predicted fiber length change.

Sensors 2 and 3 have a greater standard deviation about the predicted line. This is a result of not enough resolution. The resolution improvement factor could be increased by physically passing the fiber more times along the interaction region.

### **4.3 Reentrant Loop Photoelastic Coefficient Experiment**

The feasibility of the fiber optic reentrant loop will be determined by the accuracy with which the photoelastic coefficient can be evaluated experimentally. This is important since it is recognized that a certain amount of modal instability exists in large-core step-index fibers. Also, the photoelastic coefficient could be dependent on the number of pulse recirculations since couplers alter the modal content. The following experiment is designed to resolve these issues.

The experimental setup is shown in Figure 4.7. This setup is similar to the one in section 4.1 and indeed the fiber is secured at both points in the same fashion. The fiber is elongated from a taut position up to 2500  $\mu\text{m}$  in 500  $\mu\text{m}$  increments. The reference pulse location used here was pulse 0. The change in arrival times for pulses 1, 16, 17, 18, 19, and 20 were monitored. This experiment was repeated five times. The photoelastic coefficient was calculated using equation (3.27) for each pulse monitored for each experimental run. The averaged results are displayed in Table 4.1.

The standard deviation of the photoelastic coefficient for pulse 1 is extremely high while small standard deviations for pulses 16-20 were measured. A plausible reason for the apparent variance in the photoelastic coefficient for lower order

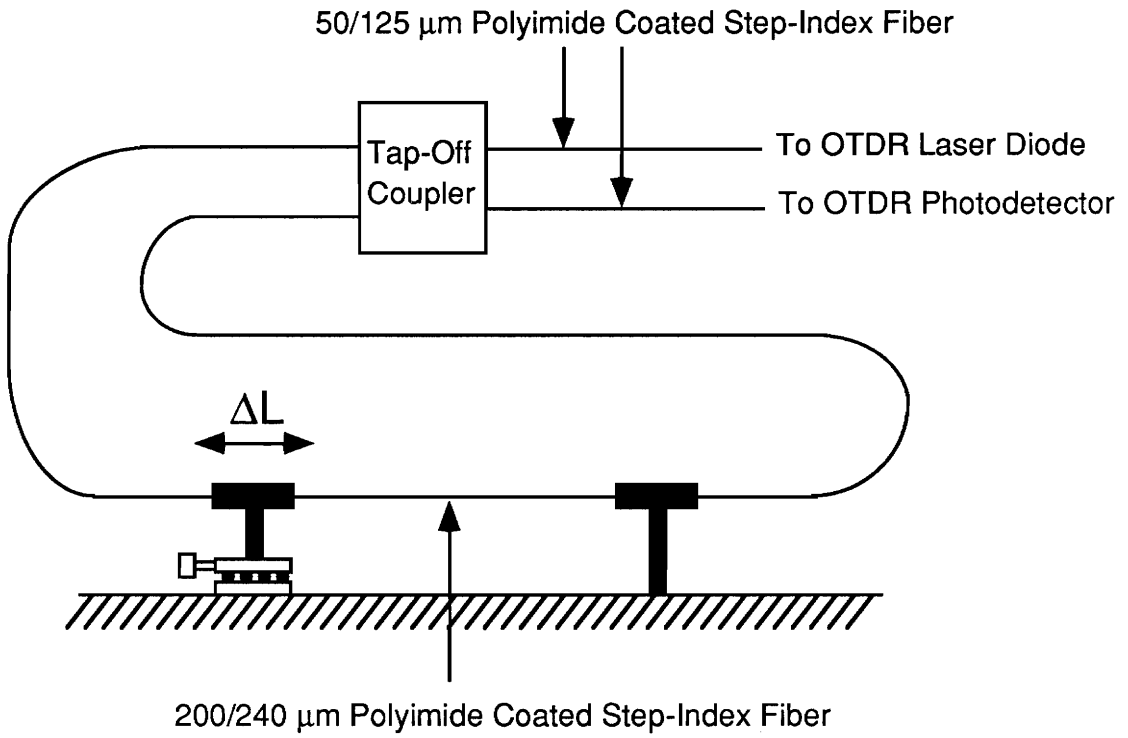


Figure 4.7. Experimental setup for the reentrant loop photoelastic coefficient determination.

Table 4.1: Reentrant Loop Photoelastic Coefficient Analysis

Pulse Recirculation Number	Photoelastic Coefficient	
	Average	Standard Deviation
1	-0.351	0.143
16	-0.211	0.029
17	-0.203	0.014
18	-0.198	0.013
19	-0.191	0.029
20	-0.209	0.021

recirculation numbers is each recirculation causes the 50/125  $\mu\text{m}$  fiber to tap off some of the higher order modes from the 200/240  $\mu\text{m}$  loop fiber. On the following recirculation, most of the lower order modes within the loop continue to recirculate, while the higher order modes from the 200/240  $\mu\text{m}$  fiber, which were tapped off onto the 50/125  $\mu\text{m}$  fiber, are detected at the receiving end. This means that, as the recirculation number increases, mainly lower order modes propagate through the 200/240  $\mu\text{m}$  sensing fiber loop. For lower circulation numbers, modal equilibrium has not yet been reached, and hence the value of the photoelastic coefficient has not stabilized. In fact, these results compare with the modally dependent photoelastic coefficient found using the ray-optics approach.

## 5.0 PRACTICAL CONSIDERATIONS

The emphasis of this thesis is to model the optical time domain strain sensor accurately and to increase its sensitivity such that its use can become practical. Strain can be measured on a quasi-distributed basis using the segmented sensor, however physically passing the fiber many times over the interaction region can be cumbersome. The reentrant loop strain sensor gives a better approach to resolution improvement, although the advantage of quasi-distributed measurements is no longer possible using a single sensing system.

The variation in determining the photoelastic coefficient could be eliminated by using single mode fibers, as this would eliminate any modal content change. This was not an option in this research effort as not enough power could be coupled into the fibers using the 850 nm wavelength multimode laser. If single mode fibers were to be used, an alternative to the tap-off coupler must be developed to obtain the proper power splitting ratio. One possible alternative is to use a single mode 2x2 coupler along with an optical amplifier within the fiber sensing loop to keep the pulse power level within the optical time domain system's received power dynamic range.

The issue that is probably most important to address is the ability to measure dynamic strains. The optical time domain system is not well suited for this application. The fastest sampling rate attained, while keeping the +/- 1 ps temporal resolution, was 3 seconds. The sensors are probably better applied to non-destructive testing and evaluation of structures. In this scenerio, strain is

sensed in the direction of the fiber sensors. Optical time domain sensors also have the unique advantage to detect the temporal location of any fiber breakage by examining the received Rayleigh backscatter from the sensor. This is useful for determining the exact location of damage.

## 6.0 CONCLUSION

The practicality of the high resolution optical time domain segmented and reentrant loop strain sensors has been shown. Among the advantages of optical time domain sensors is their large linear dynamic range. Also, the ability to make quasi-distributed measurements is novel. If quasi-distributed measurements are not required, then the fiber optic reentrant loop offers smaller size, and, for high recirculation numbers, can be modeled as accurately as the 100/140  $\mu\text{m}$  graded-index fiber.

The ray-optic model for the determination of the photoelastic coefficient was developed. Despite the simplicity of the approach, excellent comparisons have been shown between theoretically predicted values and experimentally observed coefficients. The availability of the model will help evaluate the variation in the photoelastic coefficient with different values of the Poisson ratio,  $\mu$ , and the strain-optic coefficients,  $p_{11}$  and  $p_{12}$ . It has been suggested that a single mode recirculating system would be optimal, since only the lowest order mode propagates through the fiber. Until this single mode system is developed, the ray-optics model described in this thesis will serve as a starting point for the determination of the photoelastic coefficient in step-index multimode optical time domain systems.

A more compact design of a Fresnel reflection site was also presented. The miniaturized Fresnel reflection site, measuring only 1.5 cm by 355  $\mu\text{m}$ , makes the site more flexible and easier to implement. However, if strength of the site is necessary then a more rugged design should be used.

## APPENDIX A: Derivation of Photoelastic Coefficient

The following is an analysis to determine how the time of flight of a pulse launched into a step-index, multimode optical fiber varies with modal content. The analysis will begin by differentiating equation (3.1), which describes the relation between fiber change in length,  $\Delta l_f$ , and the change in optical pulse time of flight,  $\Delta t$ , given by

$$\Delta l_f = v_g \Delta t + \frac{l_f}{v_g} \Delta v_g, \quad (\text{A.1})$$

where  $v_g$  is the group velocity of the modes travelling in the fiber core. When the fiber is subjected to an axial strain, three physical parameters of the fiber will affect the group velocity. These parameters are the fiber core radius,  $r$ , the core refractive index,  $n_1$ , and the cladding refractive index,  $n_2$ . The change in modal group velocities can be expressed as a differential summation of these effects yielding

$$\Delta v_g = \frac{\partial v_g}{\partial r} \Delta r + \frac{\partial v_g}{\partial n_1} \Delta n_1 + \frac{\partial v_g}{\partial n_2} \Delta n_2. \quad (\text{A.2})$$

Before solving equation (A.2), an expression for the group velocity will be derived in terms of familiar tabulated optical waveguide quantities, the normalized propagation constant,  $b$ , and the factor  $d(bV)/dV$ . The group velocity is given by [17]

$$v_g = \frac{d\omega}{d\beta}, \quad (\text{A.3})$$

where  $\omega$  is the operating optical frequency and  $\beta$  is the propagation constant. The normalized propagation constant,  $b$ , for each propagating mode is given by

definition to be

$$b = \frac{\beta^2/k^2 - n_2^2}{\gamma} = \frac{\beta^2 c^2}{\omega^2 \gamma} - \frac{n_2^2}{\gamma}, \quad (\text{A.4})$$

where  $c$  is the speed of light in a vacuum and  $\gamma$  represents  $(n_1^2 - n_2^2)$ . The frequency  $\omega$  expressed in terms of the normalized frequency  $V$  is given by

$$\omega = \frac{Vc}{r} \frac{1}{\sqrt{\gamma}}. \quad (\text{A.5})$$

Substituting equation (A.5) into equation (A.4) yields

$$b = \frac{\beta^2 r^2}{V^2} - \frac{n_2^2}{\gamma}. \quad (\text{A.6})$$

The factor  $d(bV)/dV$  can now be expressed as

$$\frac{d(bV)}{dV} = -\frac{\beta^2 r^2}{V^2} + \frac{2\beta r^2}{V} \frac{d\beta}{d\omega} \frac{d\omega}{dV} - \frac{n_2^2}{\gamma}, \quad (\text{A.7})$$

where

$$\frac{d\omega}{dV} = \frac{c}{r \sqrt{\gamma}}. \quad (\text{A.8})$$

Substituting equation (A.8) into equation (A.7) and solving for  $d\omega/d\beta$  yields

$$v_g = \frac{d\omega}{d\beta} = \frac{2c \sqrt{b\gamma + n_2^2}}{\gamma(b + \frac{d(bV)}{dV}) + 2n_2^2}. \quad (\text{A.9})$$

Before evaluating equation (A.2), it will be useful to define the following quantities as

$$A = \frac{\partial b}{\partial r}, B = \frac{\partial b}{\partial n_1}, C = \frac{\partial v_g}{\partial n_2}, D = \frac{\partial}{\partial r} \left[ \frac{d(bV)}{dV} \right],$$

$$E = \frac{\partial}{\partial n_1} \left[ \frac{d(bV)}{dV} \right], \text{ and } F = \frac{\partial}{\partial n_2} \left[ \frac{d(bV)}{dV} \right]. \quad (\text{A.10a-f})$$

Equation (A.2) will be examined in three separate parts with each representing the contribution of an individual physical parameter on the group velocity. The effect of the change in core radius will be examined first by taking the partial derivative of  $v_g$ , which yields

$$\frac{\partial v_g}{\partial r} = \frac{c\gamma Ak}{\beta \left( \gamma \left[ b + \frac{d(bV)}{dV} \right] + 2n_2^2 \right)} - \frac{2c\gamma (A+D) \beta}{k \left( \gamma \left[ b + \frac{d(bV)}{dV} \right] + 2n_2^2 \right)^2}. \quad (\text{A.11})$$

The change in core radius,  $\Delta r$ , due to fiber change in length is given by [1]

$$\Delta r = - \mu r \frac{\Delta l_f}{l_f}, \quad (\text{A.12})$$

where  $\mu$  is Poisson's ratio. The effect of the change in core index of refraction is found by taking the partial of equation (A.9) with respect to  $n_1$

$$\frac{\partial v_g}{\partial n_1} = \frac{kc (2bn_1 + n_1^2 B)}{\beta \left( \gamma \left[ b + \frac{d(bV)}{dV} \right] + 2n_2^2 \right)}$$

$$- \frac{2c\beta \left( \gamma (B+E) + 2n_1 \left[ b + \frac{d(bV)}{dV} \right] \right)}{k \left( \gamma \left[ b + \frac{d(bV)}{dV} \right] + 2n_2^2 \right)^2}. \quad (\text{A.13})$$

The change in core refractive index,  $\Delta n_1$ , is given by [1]

$$\Delta n_1 = -\frac{1}{2}n_1^3 \frac{\Delta l_f}{l_f} [(1 - \mu) p_{12} - \mu p_{11}] = -\frac{1}{2}n_1^3 \frac{\Delta l_f}{l_f} P, \quad (\text{A.14})$$

where  $p_{ij}$  is the strain-optic tensor. The final effect is that of the change in cladding refractive index,  $\Delta n_2$ , which is found by first taking the derivative of equation (A.9) with respect to  $n_2$  resulting in

$$\frac{\partial v_g}{\partial n_2} = \frac{kc(2n_1 - 2bn_2 - n_2^2 C)}{\beta(\gamma[b + \frac{d(bV)}{dV}] + 2n_2^2)}$$

$$- \frac{2C\beta(2n_2[2 - b - \frac{d(bV)}{dV}] - n_2^2(C + F))}{k(\gamma[b + \frac{d(bV)}{dV}] + 2n_2^2)^2}. \quad (\text{A.15})$$

As with equation (A.14), the change in cladding refractive index due to fiber change in length is given by

$$\Delta n_2 = -\frac{1}{2}n_2^3 \frac{\Delta l_f}{l_f} P, \quad (\text{A.16})$$

Substituting  $\Delta v_g$  into equation (A.1) and solving for  $\Delta t$  yields

$$\Delta t = \frac{\Delta l_f}{v_g} [1 - \frac{1}{v_g} [-\mu r \frac{\partial v_g}{\partial r} - \frac{1}{2}n_1^3 P \frac{\partial v_g}{\partial n_1} - \frac{1}{2}n_2^3 P \frac{\partial v_g}{\partial n_2}]]. \quad (\text{A.17})$$

Equation (A.17) is the desired result as it relates the fiber length change, change in fiber radius, and change in the core and cladding refractive indices to the

change in optical pulse arrival time. To make the analysis complete, equation (A.10a-f) will now be evaluated. Solving for A, B, and C yields

$$A = \frac{\partial b}{\partial r} = \frac{db}{dV} \frac{dV}{dr} = \frac{1}{r} \left[ \frac{d(bV)}{dV} - b \right], \quad (\text{A.18})$$

$$B = \frac{\partial b}{\partial n_1} = \frac{db}{dV} \frac{dV}{dn_1} = \frac{n_1}{\gamma} \left[ \frac{d(bV)}{dV} - b \right], \text{ and} \quad (\text{A.19})$$

$$C = \frac{\partial b}{\partial n_2} = \frac{db}{dV} \frac{dV}{dn_2} = \frac{-n_2}{\gamma} \left[ \frac{d(bV)}{dV} - b \right]. \quad (\text{A.20})$$

Before solving for D, E, and F, the factor  $d(bV)/dV$  in the ray optics approximation can be expressed as [18]

$$\frac{d(bV)}{dV} = 1 - \frac{u^2}{V^2} [1 - 2\kappa_l(w)] \quad (\text{A.21})$$

where

$$u^2 = r^2(k^2 n_1^2 - \beta^2), \quad (\text{A.22})$$

$$w^2 = r^2(\beta^2 - k^2 n_2^2), \text{ and} \quad (\text{A.23})$$

$$\kappa_l(w) \simeq 1 - \left( \sqrt{w^2 + l^2} + \frac{u^2}{u^2 - l^2} \right)^{-1}. \quad (\text{A.24})$$

Recognizing that  $u^2/V^2 = (1 - b)$ , equation (A.21) can be simplified to yield

$$\frac{d(bV)}{dV} = 2 - b - 2(1 - b)J, \quad (\text{A.25})$$

where

$$J = \left\{ \sqrt{V^2 b + l^2} + \frac{V^2(1-b)}{V^2(1-b) + l^2} \right\}^{-1}. \quad (\text{A.26})$$

Next, the following intermediate results will be evaluated as

$$G = \frac{\partial J}{\partial r} = -J^2 \left\{ \frac{V^2(A + \frac{2b}{l})}{2\sqrt{V^2 b + l^2}} + \frac{l^2 V^2(1-b) \left[ \frac{2}{l} - A \right]}{[V^2(1-b) + l^2]^2} \right\}, \quad (\text{A.27})$$

$$H = \frac{\partial J}{\partial n_1} = -J^2 \left\{ \frac{V^2(B + \frac{2bn_1}{\delta})}{2\sqrt{V^2 b + l^2}} + \frac{l^2 V^2(1-b) \left[ \frac{2n_1}{\gamma} - B \right]}{[V^2(1-b) + l^2]^2} \right\}, \text{ and} \quad (\text{A.28})$$

$$I = \frac{\partial J}{\partial n_2} = -J^2 \left\{ \frac{V^2(C - \frac{2bn_1}{\gamma})}{2\sqrt{V^2 b + l^2}} + \frac{l^2 V^2(1-b) \left[ -\frac{2n_2}{\gamma} - C \right]}{[V^2(1-b) + l^2]^2} \right\}. \quad (\text{A.29})$$

And finally, D, E, and F can now be expressed as

$$D = A(2J - 1) - 2(1-b)G, \quad (\text{A.30})$$

$$E = B(2J - 1) - 2(1-b)H, \text{ and} \quad (\text{A.31})$$

$$F = C(2J - 1) - 2(1-b)I. \quad (\text{A.32})$$

Now that we have expressions for A through J, the  $\Delta l$ , to  $\Delta t$  relationship of equation (A.17) is completely defined.

## APPENDIX B: C Program

```
/*
*****
/* This is a C program to acquire data using the Optoelectronics */
/* OTDR system via a GPIB interface */
/* written by Daniel D. Thomas June 1990 */
*****
*/

#include <stdio.h>
#include <math.h>
#include <stdlib.h>
#include <string.h>
#include <decl.h>
#include <graph.h>

/* Global declaration of file pointer and input variables */

FILE *fptr; /* pointer to FILE */
int otdr; /* otdr device integer */
int board; /* gpib board integer */
char clear[ ] = "CLEAR";
struct /* structure named "input" contains all */
{ /* input variables */
char sweeps[5]; /* Number of sweeps */
char time_scale[3]; /* Time scale per division */
int num_of_meas; /* Number of measurements to take */
float stability_condition; /* Maximum allowable standard deviation */
float ref_condition; /* Maximum allowable reference shift */
int pulse_flag; /* Pulse monitoring scheme flag */
int num_of_pulses; /* Number of measurment pulses */
char single_meas_pulse_pos[11]; /* Single : pulse position */
char dual_ref_pulse_pos[11]; /* Dual : reference pulse position */
char dual_meas_pulse_pos[50][11]; /* Dual : measurement positions */
int output; /* Type of output desired */
float a_coeff; /* Strain-Optic coefficient */
float alpha_coeff; /* Temperature alpha coefficient */
float beta_coeff; /* Temperature beta coefficient */
int i; /* Resolution improvement factor */
float length; /* Length of sensor */
float index; /* Group refractive index of core */
} input;

/* Main body of program */

main()
{

/* Declaration of main program variables */
```

```

char pc[ ] = "GPIB0";
char device5[ ] = "DEV5";
char repeat_flag = 'y', failure_repeat_flag = 'y', temp[10];
char extra_repeat_flag = 'r', vstemp[10];
char ch, spr, command6[50];
char command1[50] = "SWEEP ";
char command2[50] = "TIME ";
char command3[50] = "DELAY ";
char command4[30];
char command5[50] = " RSIG ";
int measurement_count = 0, count, count2, scale;
float x, scaling_factor[300], ref_sep, sd[300], square_total = 0;
float total = 0, vstotal = 0, delta[300], avg[300], vsavg[300];
float delta1[300], delta_temp[300];

#define command6 " MSIG SEND SE "
#define command7 " SEND DB "

/* Check if GPIB board is present and proper GPIB software was */
/* booted. */
if ((board = ibfind (pc)) < 0) printf("\nboard not found\n");

/* Check if OTDR processor is physically connected and turned on */
/* if ((otdr = ibfind (device5)) < 0) printf("\notdr not found\n");

/*****
/* Initailize OTDR processor by sending a series of CLEAR commands. */
/*****
poll_check();
ibwrt(otdr,clear,5);
poll_check();
ibwrt(otdr,clear,5);
poll_check();
ibwrt(otdr,clear,5);
/*****

setup(); /* Call setup subroutine */
scale = atoi(input.time_scale); /* Define integer value to determine */
/* proper scaling factor to all output */
/* is in picoseconds. */

/*****
/* Send commands to set sweeps and time scale on OTDR. */
/*****
strcat(command1,input.sweeps); /* create command string to set sweeps */
strcat(command2,input.time_scale); /* create command to set time scale */
poll_check(); /* check OTDR status byte for a ready response */
poll_check();
ibwrt(otdr,command2,7); /* send sweep command string */
poll_check();
ibwrt(otdr,command1,10); /* send time scale command string */

```

```

poll_check();
ibwrt(otdr,command2,7); /* reduntantly send sweep command string */
poll_check();
ibwrt(otdr,command1,10); /* reduntantly send time scale command string */
poll_check();
/*****
/*****
/* Single pulse monitoring logic */
/*****
if (input.pulse_flag == 1)
{
    strcat(command3,input.single_meas_pulse_pos);
    while (repeat_flag != 'e')
    {
total = 0.0;
vstotal = 0.0;
square_total = 0.0;
measurement_count++;
clearscreen();
poll_check();
ibwrt(otdr,command3,16);
poll_check();
pulse_on_screen();
ibwrt(otdr,command5,8);
poll_check();
ibwrt(otdr,clear,5);
printf("\n\n\n\n Press any key to begin taking measurements.");
ch = getche();
for (count=0; count<input.num_of_meas; count++)
{
    strcpy(temp,"");
    strcpy(vstemp,"");
    ibwrt(otdr,command6,20);
    poll_check();
    ibrd(otdr,temp,10);
    if (scale == 3)
        deltat[count] = atof(temp);
    else
        deltat[count] = 1000*atof(temp);
    total = total + deltat[count];
    square_total = square_total + pow(deltat[count],2);
    ibwrt(otdr,command7,10);
    poll_check();
    ibrd(otdr,vstemp,10);
    scaling_factor[count] = atof(vstemp);
    vstotal = vstotal + scaling_factor[count];
}
avg[measurement_count] = total/input.num_of_meas;
vsavg[measurement_count] = vstotal/input.num_of_meas;
x = (input.num_of_meas*square_total - pow(total,2));

```

```

x = x/(input.num_of_meas*(input.num_of_meas - 1));
sd[measurement_count] = pow(fabs(x),.5);
poll_check();
ibwrt(odr,clear,5);
clearscreen();
printf("      Single Pulse Analysis\n");
for (count=0; count<input.num_of_meas; count++)
    {printf("\n Measurement Pulse Shift = %f ps",
    deltat[count]);}
if (sd[measurement_count] >= input.stability_condition)
    printf("\n\n WARNING - Stability Condition Failed!");
printf("\n\n Average of Pulse Shifts = %f ps",
avg[measurement_count]);
printf("\n Standard Deviation of Pulse Shifts = %f ps\n",
sd[measurement_count]);
if (input.output == 2)
    {
    deltat[measurement_count] = avg[measurement_count]*
    3*pow(10,-4)/(input.index*input.i*(1+input.a_coeff));
    printf(" Fiber Length Change = %f m\n",
    deltat[measurement_count]);
    }
if (input.output == 3)
    {
    delta_temp[measurement_count] = 3*pow(10,-4)*
    avg[measurement_count]/(input.i*input.length*
    (input.beta_coeff+(input.alpha_coeff*input.index)));
    printf(" Temperature Change = %f Celcius\n",
    delta_temp[measurement_count]);
    }
for (count=0; count<input.num_of_meas; count++)
    {printf("\n Loss in db Between Reference and Measured Pulse = %f",
    scaling_factor[count]);}
printf("\n Average of Loss = %f",
vsavg[measurement_count]);
printf("\n\n Type any key to take another series of measurements");
printf("\n or 'e' to exit: \n");
repeat_flag = getche();
}
}
/*****
/*****
/* Dual pulse monitoring logic. */
/*****
if (input.pulse_flag == 2)
    {
    strcat(command3,input.dual_ref_pulse_pos);
    while (repeat_flag != 'e')
    {
for (count2=0; count2<input.num_of_pulses; count2++)

```

```

{
extra_repeat_flag = 'r';
while (extra_repeat_flag == 'r')
{
total = 0.0;
vstotal = 0.0;
square_total = 0.0;
measurement_count++;
clearscreen();
poll_check();
ibwrt(otdr,command3,16);
poll_check();
pulse_on_screen();
poll_check();
ibwrt(otdr,command5,8);
strcpy(command4,"");
strcpy(command4,"DELAY ");
strcat(command4,input.dual_meas_pulse_pos[count2]);
poll_check();
ibwrt(otdr,command4,16);
poll_check();
pulse_on_screen();
for (count=0; count<input.num_of_meas; count++)
{
strcpy(temp,"");
strcpy(vstemp,"");
poll_check();
ibwrt(otdr,command6,20);
poll_check();
ibrd(otdr,temp,10);
if (scale == 3)
deltat[count] = atof(temp);
else
deltat[count] = 1000*atof(temp);
total = total + deltat[count];
square_total = square_total + pow(deltat[count],2);
ibwrt(otdr,command7,10);
poll_check();
ibrd(otdr,vstemp,10);
scaling_factor[count] = atof(vstemp);
vstotal = vstotal + scaling_factor[count];
}
poll_check();
ibwrt(otdr,command3,16);
poll_check();
pulse_on_screen();
poll_check();
ibwrt(otdr,command6,20);
strcpy(temp,"");
poll_check();
ibrd(otdr,temp,10);

```

```

if (scale == 3)
    ref_sep = atof(temp);
else
    ref_sep = 1000*atof(temp);
avg[measurement_count] = total/input.num_of_meas;
vsavg[measurement_count] = vstotal/input.num_of_meas;
x = (input.num_of_meas*square_total - pow(total,2));
x = x/(input.num_of_meas*(input.num_of_meas - 1));
sd[measurement_count] = pow(fabs(x),.5);
poll_check();
ibwrt(otdr,clear,5);
clearscreen();
printf("      Measurement Pulse %d Analysis\n",count2+1);
for (count=0; count<input.num_of_meas; count++)
    {printf("\n Reference to Measurement Pulse Separation = %f ps",
    deltat[count]);}
if (sd[measurement_count] >= input.stability_condition)
    printf("\n\n WARNING - Stability Condition Failed!");
if (fabs(ref_sep) >= input.ref_condition)
    printf("\n\n WARNING - Reference Pulse Condition Failed!");
printf("\n\n Average of Pulse Separations = %f ps",
avg[measurement_count]);
printf("\n Standard Deviation of Pulse Separations = %f ps",
sd[measurement_count]);
printf("\n Reference Pulse Shift = %f ps\n",ref_sep);
if (input.output == 2)
    {
    deltal[measurement_count] = (avg[measurement_count]-avg[1])*
    3*pow(10,-4)/(input.index*input.i*(1+input.a_coeff));
    printf(" Fiber Length Change = %f m\n",
    deltal[measurement_count]);
    printf("\n avg[1] = %f \n",avg[1]);
    }
if (input.output == 3)
    {
    if (measurement_count == 1)
        delta_temp[1] = 0.0;
    else
        {
        delta_temp[measurement_count] = 3*pow(10,-4)*
        (avg[measurement_count]-avg[1])/(input.i*input.length*
        (input.beta_coeff+(input.alpha_coeff*input.index)));
        }
    printf(" Temperature Change = %f Celcius\n",
    delta_temp[measurement_count]);
    }
for (count=0; count<input.num_of_meas; count++)
    {printf("\n Loss in db Between Reference and Measured Pulse = %f",
    scaling_factor[count]);}
printf("\n Average of Loss = %f",
vsavg[measurement_count]);

```



```

printf("\n Number of sweeps the OTDR processor will average.");
printf("\n (Must be a power of 2 from 2-65536) : %s",input.sweeps);
printf("\n Time scale (Time/Division) for oscilloscope to display pulse.");
printf("\n Use 3 for 50 Picoseconds/Division");
printf("\n Use 4 for 100 Picoseconds/Division");
printf("\n Use 5 for 200 Picoseconds/Division");
printf("\n Use 6 for 500 Picoseconds/Division : %s",input.time_scale);
printf("\n Number of measurements to be taken");
printf("\n for each run. : %d",input.num_of_meas);
printf("\n Maximum standard deviation of measured");
printf("\n pulse locations before user is flagged : %f ps",
input.stability_condition);
printf("\n Maximum shift of reference pulse's location before");
printf("\n user is flagged : %f ps",input.ref_condition);
if (input.pulse_flag == 1)
printf("\n Time delay of measurement pulse : %s",
input.single_meas_pulse_pos);
if (input.pulse_flag == 2)
{
printf("\n Time delay of reference pulse : %s",
input.dual_ref_pulse_pos);
for (count=0; count<input.num_of_pulses; count++)
printf("\n Time delay of measurement pulse %d : %s",
count+1, input.dual_meas_pulse_pos[count]);
}
if (input.output == 1)
printf("\n Output parameter : Time");
if (input.output == 2)
{
printf("\n Output parameter : Strain");
printf("\n Photoelastic coefficient : %f",input.a_coeff);
printf("\n Resolution improvement factor : %d",input.i);
printf("\n Group refractive index of fiber : %f",input.index);
}
if (input.output == 3)
{
printf("\n Output parameter : Temperature");
printf("\n Alpha coefficient : %f",input.alpha_coeff);
printf("\n Beta coefficient : %f",input.beta_coeff);
printf("\n Resolution improvement factor : %d",input.i);
printf("\n Length of sensing fiber (meters) : %f",input.length);
printf("\n Group refractive index of fiber : %f",input.index);
}
printf("\n\n Type any key to return to Main Menu: ");
return_ch = getch();
fclose(fp);
}
/*****
/*****/

```

```

/* Run main program using setup data. */
/*****
if (menu_ch == '2')
{
if( (fptr = fopen("setup1.dat","rb"))==NULL )
printf("/n Can't open file setup1.dat/n");
fread(&input,sizeof(input),1,fptr);
fclose(fptr);
return;
}
*****/

/*****
/* User entering new setup data logic. */
*****/
if (menu_ch == '3')
{
if( (fptr = fopen("setup1.dat","wb"))==NULL )
printf("/n Can't open file setup1.dat/n");
printf("\n Enter number of sweeps the OTDR processor will average.");
printf("\n (Must be a power of 2 from 2-65536) : ");
scanf("%s",input.sweeps);
printf("\n\n Enter time scale (Time/Division) for oscilloscope ");
printf("\n to display pulse.");
printf("\n Use 3 for 50 Picoseconds/Division");
printf("\n Use 4 for 100 Picoseconds/Division");
printf("\n Use 5 for 200 Picoseconds/Division");
printf("\n Use 6 for 500 Picoseconds/Division : ");
scanf("%s",input.time_scale);
printf("\n\n Enter the number of measurements to be taken");
printf("\n for each run : ");
scanf("%d",&input.num_of_meas);
printf("\n\n Enter the maximum allowable standard deviation");
printf("\n of measured pulse locations before user is flagged (ps) : ");
scanf("%f",&input.stability_condition);
printf("\n\n Enter the maximum shift of reference pulse's location");
printf("\n before user is flagged (ps) : ");
scanf("%f",&input.ref_condition);
while (error_flag != 'n') /* check if user entered a proper response */
{
error_flag = 'n';
printf("\n\n Enter the pulse monitoring scheme (1=single, 2=dual) : ");
scanf("%d",&input.pulse_flag);
if (input.pulse_flag != 1 && input.pulse_flag != 2)
{
printf("\n ERROR - Improper choice!\n");
error_flag = 'y';
}
}
if (input.pulse_flag == 1)
{

```

```

printf("\n\n Enter the position of the pulse to be monitored;");
printf("\n\n must end with a U for microseconds or a N for nanoseconds : ");
scanf("%s",input.single_meas_pulse_pos);
}
if (input.pulse_flag == 2)
{
printf("\n\n Enter the position of the reference pulse to be monitored;");
printf("\n\n must end with a U for microseconds or a N for nanoseconds : ");
scanf("%s",input.dual_ref_pulse_pos);
printf("\n\n Enter the number of measurement pulses to be monitored.");
printf("\n\n (i.e. How many reflection sites to be monitored.) : ");
scanf("%d",&input.num_of_pulses);
for (count=0; count<input.num_of_pulses; count++)
{
printf("\n\n Enter the position of measurement pulse %d to be monitored.",
count+1);
printf("\n\n must end with a U for microseconds or a N for nanoseconds : ");
scanf("%s",input.dual_meas_pulse_pos[count]);
}
}
if (input.num_of_pulses>1 && input.pulse_flag==2)
{
input.output = 1;
printf("\n\n NOTE : Output has been automatically set to TIME.\n");
}
else
{
printf("\n\n Enter the desired output parameter.");
printf("\n\n (1=time, 2=strain, 3=temperature) : ");
scanf("%d",&input.output);
}
if (input.output == 2)
{
printf("\n\n Enter the photoelastic coefficient : ");
scanf("%f",&input.a_coeff);
printf("\n\n Enter the resolution improvement factor");
printf("\n\n (must be an integer) : ");
scanf("%d",&input.i);
printf("\n\n Enter the group refractive index of fiber : ");
scanf("%f",&input.index);
}
if (input.output == 3)
{
printf("\n\n Enter the alpha coefficient : ");
scanf("%f",&input.alpha_coeff);
printf("\n\n Enter the beta coefficient : ");
scanf("%f",&input.beta_coeff);
printf("\n\n Enter the resolution improvement factor");
printf("\n\n (must be an integer) : ");
scanf("%d",&input.i);
printf("\n\n Enter the length of sensing fiber (meters) : ");
}

```



```
ibsic(board);
ibsre(board,0);
ibsic(board);
printf("\n Adjust ODTR's Volts/Division and vertical position");
printf("\n so entire pulse appears on oscilloscope screen.");
printf("\n WARNING - Do not adjust gain after initial setting");
printf("\n          as this will corrupt results!");
printf("\n\n (Hit any key when ready)\n");
ch = getche();
ibsre(board,1);
}
```

## REFERENCES

1. C. D. Butter and G. B. Hocker, "Fiber Optics Strain Gauge," *Applied Optics*, vol. 17, no. 18, pp. 2862-2869, 15 September 1978.
2. A. J. Rogers, "Distributed Optical-Fibre Sensors," *Journal of Applied Physics*, vol. 19, pp. 2237-2255, December 1986.
3. G. D. Pitt, "Fiber Optic Sensors," *Electrical Communication*, vol. 24, no. 2, pp. 102-106, 1982.
4. P. S. Loveley, "Researchers Meet OTDR Challenges," *Laser Focus*, vol. 24, pp. 139-141, December 1988.
5. Opto-Electronics Inc., "Operating Manual: Millimeter Resolution OTDR System," September 1988.
6. Opto-Electronics Inc., "Picosecond Fibre Optic System Operations Manual," November 1984.
7. D. Cox, D. D. Thomas, K. Reichard, D. K. Lindner, and R. O. Claus, "Vibration Control of a Flexible Beam Using a Distributed Fiber Optic Sensor," *Proc. of the 28th IEEE Conf. on Decision and Control*, pp. 2685-2686, December 1989.
8. J. N. Blake, S. Y. Huang, and B. Y. Kim, "Elliptical Core Two-Mode Fiber Strain Gauge," *SPIE*, August 1987.
9. R. E. Love, "The Strength of Optical Waveguide Fibers," *Proc. SPIE Conf.*, vol. 77, Reston, VA, 1976.
10. R. D. Maurer, "Strength of Fiber Optical Waveguides," *Applied Physics Letters*, vol. 27, no. 4, 1975.

11. B. D. Zimmermann, "High Resolution Optical Time Domain Reflectometry and its Applications," M. S. Thesis, Virginia Tech, 1988.
12. A. Bértholds and R. Dandliker, "Determination of the Individual Strain-Optic Coefficients in Single-Mode Fibers," *J. Lightwave Tech.*, vol. 6, no. 1, pp. 17-20, 1988.
13. M. Nazarathy and S. A. Newton, "Rayleigh Backscattering in Optical Fiber Recirculating Delay Lines," *Applied Optics*, vol. 25, no. 7, pp. 1051-1055, 1986.
14. S. A. Newton, R. S. Howland, K. P. Jackson, and H. J. Shaw, "High Speed Pulse Train Generation Using Single-Mode Fibre Recirculating Delay Lines," *Electronics Letters*, vol. 19, no. 19, pp. 756-758, 1983.
15. S. A. Newton et. al., "Measured Backscatter Signature of a Fiber Recirculating Delay Line," *Applied Optics*, vol. 25, no. 12, pp. 1879-1881, 1986.
16. F. P. Beer and E. R. Johnston, Jr., *Mechanics of Materials*, McGraw-Hill, New York, 1981.
17. W. B. Jones, Jr. , *Introduction to Optical Fiber Communication Systems*, Holt, Rinehart and Winston, Inc., New York, 1988.
18. I. A. White and C. Pask, "Effect of Goos-Hanchen Shifts on Pulse Widths in Optical Waveguides," *Applied Optics*, vol. 16, pp.2353-2355, 1977.

## VITA

Daniel Douglas Thomas was born in Fredricksburg, Virginia, on September 28, 1965 and attended King George High School in King George, Virginia. He received the Bachelor of Science in Electrical Engineering degree from Virginia Polytechnic Institute and State University in July 1988. While pursuing the B. S. degree, he successfully completed the cooperative education program with Naval Surface Warfare Center in Dahlgren, Virginia. He then went on to pursue his Master of Science degree in Electrical Engineering at Virginia Polytechnic Institute and State University, which was awarded in August 1990.